

## RESEARCH ARTICLE

# Reelin cells and sex-dependent synaptopathology in autism following postnatal immune activation

Maryam Ardanan<sup>1,2</sup> | Tetyana Chumak<sup>1</sup> | Alexandra Quist<sup>1</sup> | Eva Hermans<sup>1,3</sup> | Ali Hoseinpoor Rafati<sup>2</sup> | Giacomo Gravina<sup>1</sup> | Seyedeh Marziyeh Jabbari Shiadeh<sup>1,2</sup> | Pernilla Svedin<sup>1</sup> | Setareh Alabaf<sup>1</sup> | Brian Hansen<sup>4</sup> | Gregers Wegener<sup>2</sup> | Lars Westberg<sup>5</sup> | Carina Mallard<sup>1</sup>

<sup>1</sup>Department of Physiology, Institute of Neuroscience and Physiology, Sahlgrenska Academy, University of Gothenburg, Gothenburg, Sweden

<sup>2</sup>Department of Clinical Medicine, Translational Neuropsychiatry Unit, Aarhus University, Aarhus, Denmark

<sup>3</sup>Department of Developmental Origins of Disease, Utrecht Brain Center and Wilhelmina Children's Hospital, Utrecht University, Utrecht, Netherlands

<sup>4</sup>Department of Clinical Medicine, Center of Functionally Integrative Neuroscience-SKS, Aarhus University, Aarhus, Denmark

<sup>5</sup>Department of Pharmacology, Institute of Neuroscience and Physiology, Sahlgrenska Academy, University of Gothenburg, Gothenburg, Sweden

## Correspondence

Carina Mallard, Department of Physiology, Institute of Neuroscience and Physiology, Sahlgrenska Academy, University of Gothenburg, Box 432, SE-405 30 Gothenburg, Sweden.  
Email: [carina.mallard@neuro.gu.se](mailto:carina.mallard@neuro.gu.se)

## Funding information

National Institute of Health, Grant/Award Numbers: R01 NS103483, R01 HL139685; Swedish Brain Foundation, Grant/Award Number: FO2019-0270; Public Health Service at the Sahlgrenska University Hospital, Grant/Award Number: ALFGGB-722491; Åhlen Foundation; Swedish Research Council, Grant/Award Number: VR-2017-01409; Wilhelm och Martina Lundgrens Vetenskapsfond; Frimurare Barnhusdirektionen; Axel Tielmans Foundation, Grant/Award Number: 2020-00559; HKH Kronprinsessan Lovisas Foundation; Magn. Bergvalls Foundation, Grant/Award Number: 2020-03756; Mary von Sydows Foundation, Grant/Award Number: 2020-3420; Lundbeck Foundation, Grant/Award Number: R322-2019-2721

**Background and Purpose:** Autism spectrum disorders (ASD) are heterogeneous neurodevelopmental disorders with considerably increased risk in male infants born pre-term and with neonatal infection. Here, we investigated the role of postnatal immune activation on hippocampal synaptopathology by targeting Reelin<sup>+</sup> cells in mice with ASD-like behaviours.

**Experimental Approach:** C57/Bl6 mouse pups of both sexes received lipopolysaccharide (LPS, 1 mg·kg<sup>-1</sup>) on postnatal day (P) 5. At P45, animal behaviour was examined by marble burying and sociability test, followed by ex vivo brain MRI diffusion kurtosis imaging (DKI). Hippocampal synaptogenesis, number and morphology of Reelin<sup>+</sup> cells, and mRNA expression of trans-synaptic genes, including neurexin-3, neuroligin-1, and cell-adhesion molecule nectin-1, were analysed at P12 and P45.

**Key Results:** Social withdrawal and increased stereotypic activities in males were related to increased mean diffusivity on MRI-DKI and overgrowth in hippocampus together with retention of long-thin immature synapses on apical dendrites, decreased volume and number of Reelin<sup>+</sup> cells as well as reduced expression of trans-synaptic and cell-adhesion molecules.

**Conclusion and Implications:** The study provides new insights into sex-dependent mechanisms that may underlie ASD-like behaviour in males following postnatal immune activation. We identify GABAergic interneurons as core components of

**Abbreviations:** a/p, the area per test point; ASD, autistic spectrum disorders; ASF, area sampling fraction; CA, cornu ammonis sectors; DKI, diffusion kurtosis imaging; EPI, echo planar imaging; GCL, granular cell layer; HSF, height sampling fraction; Iba1, ionized calcium binding adaptor molecule 1; MD, mean diffusivity; MK, mean kurtosis; NLGN, neuroligin; NRXN, neurexin; P, postnatal day; PIA, postnatal immune activation; Poly(I:C), polyinosinic:polycytidylic acid; RARE, rapid imaging with refocused echoes; SI, sociability index; SR, stratum radiatum; SSF, section sampling fraction; T, the section thickness; TE, echo time; TR, repetition time;  $\Sigma P$ , the total number of the points hitting the region of interest;  $\Sigma Q$ , the total number of counted cells.

This is an open access article under the terms of the [Creative Commons Attribution-NonCommercial-NoDerivs](https://creativecommons.org/licenses/by-nc-nd/4.0/) License, which permits use and distribution in any medium, provided the original work is properly cited, the use is non-commercial and no modifications or adaptations are made.

© 2022 The Authors. *British Journal of Pharmacology* published by John Wiley & Sons Ltd on behalf of British Pharmacological Society.

dysmaturation of excitatory synapses in the hippocampus following postnatal infection and provide cellular and molecular substrates for the MRI findings with translational value.

#### KEYWORDS

autism, MRI diffusion kurtosis, neonatal infection, preterm, Reelin, synaptogenesis

## 1 | INTRODUCTION

Preterm birth and its associated complications are among the most serious global health issues that modern society faces (Blencowe et al., 2013; Strunk et al., 2014). Particularly, extreme prematurity (<28 gestational weeks) is associated with a substantially elevated risk of neurodevelopmental problems, including up to 41% for autistic spectrum disorders (ASD) (Hagberg et al., 2012, 2015; Moore et al., 2012). A recent large network study in the USA showed that the prevalence of ASD is significantly higher in boys (23.4 per 1000) than girls (5.2 per 1000) (Christensen et al., 2019). There are also distinct sex-dependent phenotypic characteristics showing that autistic females have significantly lower internalizing and anxiety problems than ASD males (Harrop et al., 2018; Prosperi et al., 2020). Individuals with ASD show overgrowth of brain regions, such as cornu ammonis sectors (CA) 1–3 of the hippocampus, already at 6 months of age, suggesting that ASD manifests at an early age (Li et al., 2019). Identifying pathophysiological and behavioural differences between males and females with autism is crucial for understanding the aetiology and may help in the early diagnosis of autism (Little et al., 2017).

Besides a strong genetic component underlying ASD, environmental factors are important (Hallmayer et al., 2011; Taylor et al., 2020). Among environmental factors, postnatal infection occurs in 20%–65% of very premature infants (Strunk et al., 2014), a population which is highly associated with neurodevelopmental abnormalities later in life (Cheong et al., 2017). It has also been suggested that the combination of preterm birth and susceptibility genes makes infants more vulnerable to environmental factors such as infection after birth and contribute to autism pathogenesis (Vargas et al., 2005). In support of the inflammation hypothesis, blood monocytes from children with ASD demonstrate distinct cytokine responses following activation of the innate immune system (Enstrom et al., 2010). An array of rodent models has been developed to explore the link between altered neuro-immune interactions and ASD. In these models, **toll-like receptor** (TLR) activation is frequently used to trigger the immune response (Ardalan et al., 2019). Prenatal and postnatal administration of lipopolysaccharide (LPS), a **TLR-4** agonist which mimics Gram-negative bacterial infection (Alexander & Rietschel, 2001), was shown to induce ASD-like behaviour in animals, especially in males (Basta-Kaim et al., 2015; Custódio et al., 2018). It has also been reported that following maternal exposure to the **TLR-3** agonist **polyinosinic:polycytidylic acid** (poly(I:C)), a viral mimic, male offspring display ASD-like behaviour (Malkova et al., 2012). While

### What is already known

- Postnatal infection in premature infants increases the risk of autism.
- Deficit in brain levels of reelin is a potential biomarker for autism.

### What does this study add

- Sex-dependent deficiency in Reelin+ cells contributes to autistic like behaviour in mice.
- Defective Reelin+ cell development may affect genes encoding transsynaptic adhesion proteins.

### What is the clinical significance

- Reelin may represent a promising therapeutic target in autism.

inflammation and prematurity have emerged as joint driving forces in ASD, due to the heterogeneous nature of autism, conclusive evidence for aetiology and pathogenesis has yet to be established.

Alterations in neuronal plasticity have been implicated in ASD neuropathology. Of particular relevance for the regulation of neuronal plasticity are genes encoding trans-synaptic adhesion proteins, including presynaptic neuroligins (NRXNs), postsynaptic neuroligins (NLGNs), and cellular adhesion molecules, including Nectin-1 (Mandai et al., 2015). These proteins affect various aspects of synapse biology, including synaptogenesis, synaptic transmission, remodelling, and maturation (Ichtchenko et al., 1995; Kwon et al., 2012). NRXN3 and NLGN1 mutations have been associated with ASD (Glessner et al., 2009; Tejada et al., 2019; Vaags et al., 2012; Yuan et al., 2018) by regulating differentiation of excitatory and inhibitory synapses (Varghese et al., 2017). Importantly, Nectin-1 regulates dendritic spine density and inhibition of Nectin-1 results in increased number of synapses in the hippocampus (Lim et al., 2012; Mizoguchi et al., 2002). Reelin, an extracellular matrix protein expressed by a population of

GABAergic Cajal Retzius (CR) interneurons, is essential for synaptic plasticity through affecting dendrites and dendritic spine development. Reelin-signalling regulates presynaptic and postsynaptic structure/function by impinging trans-synaptic adhesion proteins such as NLGN, NRXN, and Nectin-1. Deficits in brain levels of reelin mRNA have been reported in ASD cases, and it has been studied as a potential biomarker for autism (Fatemi, 2002; Lammert & Howell, 2016; Persico et al., 2001; Zhang et al., 2002) and, in mice, offspring from mothers treated with poly (I:C) showed reduced number of reelin+ cells in the hippocampus (Harvey & Boksa, 2012). However, despite the importance of reelin-signalling in synapse plasticity and ASD, it is unknown how adverse early postnatal life experience affects these pathways and how it is related to sex-dependent autistic-like behaviours. Therefore, this study aimed to explore sex-dependent effects of postnatal immune activation (PIA) on microstructure magnetic resonance imaging (MRI) parameters, Reelin+ cells, and trans-synaptic adhesion proteins in connection with synapse plasticity in the hippocampus in an animal model of postnatal infection with ASD-like phenotype. Importantly, we investigated neuropathological changes at an early age and later in adolescence to evaluate the impact of PIA on brain development over time.

## 2 | METHODS

The data and statistical analysis comply with the recommendations of the *British Journal of Pharmacology* on experimental design and analysis in pharmacology (Curtis et al., 2018). Studies were designed to generate groups of equal size, using randomization and blinded analysis.

### 2.1 | Materials

C57Bl/6J wild-type (WT) mice were purchased from Janvier Labs (Le Genest-Saint-Isle, France) and Charles River Laboratories (Sulzfeld, Germany) and fed standard laboratory chow diet (B&K, Solna, Sweden); lipopolysaccharide (LPS, #423, List Biological Laboratories, Campbell, CA, USA); saline (Sigma Aldrich, St. Louis, MO, USA); **pentobarbital** (Pentacour UK); 6% buffered formaldehyde (Histofix; Histolab products AB, Västra Frölunda, Sweden); isopentane (Sigma Aldrich, USA); cryostat (Leica, CM 3050 S, Germany); FD Rapid Golgi Stain TM Kit (FD Neuro Technologies, Inc., Columbia, MD, USA); Vibratome (Leica, VT1200S Semiautomatic Vibrating Blade Microtome, Wetzlar, Germany); thionin solution (Sigma T3387, USA); phosphate-buffered saline (Gibco Invitrogen, Waltham, MA, USA); target retrieval solution (Dako, Glostrup, Denmark); 0.02% Triton-X-100 (PBS-T, Sigma Aldrich, USA); rabbit anti-ionized calcium binding adaptor molecule 1 (Iba1) (019-19741, Wako, Japan); anti-reelin (ab78540, RRID:AB\_1603148); goat-anti-rabbit antibody (Vector Laboratories, Olean, NY, USA); ABC elite solution (Vector Laboratories, USA); 3,30-diaminobenzidine solution (Acros Organics, Geel, Belgium); gelatin-coated slides (Sigma Aldrich, USA), digital camera (Leica DFC

295, Germany); newCAST™ software (Visopharm, Hørsholm, Denmark); Nanodrop (2000/2000c, Thermo Scientific, Rockford, IL, USA); QuantiTect Reverse Transcription Kit (Qiagen, USA); QuantiFast SYBR Green PCR Master Mix (Qiagen, USA); PCR primers (Qiagen, USA), LightCycler 480 (Roche, Sweden); Quant-IT OliGreen ssDNA Assay kit (Fisher Scientific, Sweden).

### 2.2 | Animals and induction of postnatal immune activation (PIA)

Animal studies are reported in compliance with the ARRIVE guidelines (Percie du Sert et al., 2020) and with the recommendations made by the *British Journal of Pharmacology* (Lilley et al., 2020). C57Bl/6J WT mice were purchased from Janvier Labs (Le Genest-Saint-Isle, France) and Charles River Laboratories (Sulzfeld, Germany) and were bred in the animal facility at the University of Gothenburg (Experimental Biomedicine, University of Gothenburg). Mice were housed with a normal 12-h light/dark cycle (lights on at 06:00) and ad libitum access to standard laboratory chow diet (B&K, Solna, Sweden) and drinking water in a temperature-controlled environment (20–22°C). All animal experiments were approved by the Gothenburg Animal Ethical Committee (No 663/2017 with amendment Dnr 5.8.18-14322/2018). Mice of both sexes were used. Sex was established by visual inspection. In each experimental group, mice were obtained from at least three different litters. PIA was induced in male and female mice by a single intraperitoneal injection of LPS (1 mg·kg<sup>-1</sup>, #423, List Biological Laboratories, Campbell, CA, USA), a well-established animal model, on postnatal day (P) 5 to study effects of peripheral inflammation on brain function (Smith et al., 2014). This age in mice represents a critical brain developmental stage equivalent to preterm human infants (Semple et al., 2013). Control animals received an equal volume of saline (Sigma Aldrich, St. Louis, MO, USA). The experiments included two follow up time points: 7 days after injection (P12) and 45 ± 5 days after injection (P45 ± 5), corresponding to paediatric and adolescent age respectively. The P12 time point was studied as it corresponds to a stage in mouse brain development with high rate of brain growth, including gliogenesis and increasing axonal and dendritic density, and with significant brain plasticity activity (Semple et al., 2013; Watson et al., 2006), neurodevelopmental processes believed to be important in ASD (Carlezon et al., 2019; Fereshetyan et al., 2021). Accordingly, there were eight groups, with equal numbers of male and female mice in each group, for each parameter studied. After weaning (P23), the mice were separated based on sex and kept in standard conditions in the animal house (five mice from the same sex in each cage).

### 2.3 | Behavioural tests

Male and female mice were evaluated at P45 ± 5 ( $n = 10$  per treatment group per sex) for stereotypic and repetitive behaviour (marble burying test, self-grooming), sociability, and interest in social novelty

(three-chamber test). Before the initiation of behavioural tests, mice were allowed to acclimatize to the test room for 1 h. For each mouse, behavioural tests were performed at the same time every day (9 AM–4 PM) at 60 lux illumination level, starting with the marble-burying test followed by the three-chamber test with a resting time of 30 min between tests. Four mice from the same sex were tested per day. Test chamber and marbles were cleaned with 70% alcohol between each mouse.

### 2.3.1 | Marble burying test

The test was performed according to the Deacon protocol (Deacon, 2006). Briefly, 20 glass marbles (1.5 cm in diameter) were placed on the top of the bedding (in five rows of four marbles) in a Plexiglas box (32 cm [length] × 30 cm [width] × 18 cm [height]) with 5-cm bedding. Each mouse was placed in the box for 30 min, and at the end of the test, the number of buried marbles was counted. The criterion to count marbles as buried was that they were covered at least to 50% by bedding.

### 2.3.2 | Three-chamber test

Mouse sociability was examined as previously described (Yang et al., 2011) with minor modifications. Briefly, a stimulus mouse (sex- and age-matched with no previous contact with the test mouse) was selected from a cage of separately reared mice. The stimulus mouse was habituated by being placed inside a pencil cup for 30 min once per day for 2 days prior to the beginning of the test. On the day of testing, both the stimulus mouse and the test mouse were habituated to the testing room for 1 h prior to the start of behavioural tasks. The size of the chambers were: middle chamber (25 cm height × 18.7 cm length × 19.5 cm width), chamber 1 (25 cm height × 19.5 cm width × 19.5 cm length), and chamber 2 (25 cm height × 19.5 cm width × 19.5 cm length), with the overall dimensions of the box being 25 cm (height) × 19.5 cm (width) × 57.7 cm (length). Between the chambers, there was a 1-cm-wide gap which could be closed or opened during testing. The size of the pencil cup was 10 cm in height with a diameter of 8.4 cm at the bottom. The following test procedure was employed: (1) The test mouse was placed for 10 min in the middle chamber with closed gaps (habituation step); (2) the gaps between chambers were opened, and the test mouse allowed to explore all three chambers freely for 10 min (exploration step); (3) the stimulus mouse was placed inside an empty pencil cup in one of the chambers, and in the other chamber, an identical empty pencil cup was placed and the test mouse was allowed to freely explore all three chambers for 10 min; (4) the test mouse was returned to its resting cage. For the test mouse, the following parameters were scored by a blinded researcher: (1) time spent in the empty pencil cup chamber, (2) time spent in the stimulus mouse chamber, (3) time spent sniffing the empty cup or the “stimulus mouse” cup, (4) time spent in the middle chamber, and (5) number of crossings between the chambers to test

the locomotor activity. Quantification of social behaviours was performed manually by a researcher blinded to the groups of test mice. The sociability index (SI) was calculated as (time exploring social chamber time – exploring non-social chamber)/(time exploring social chamber + time exploring non-social chamber) as described (Haida et al., 2019). Self-grooming behaviour was scored for 10 min in the second step of the test, while the mouse was freely exploring the three chambers.

## 2.4 | Tissue processing for histological, immunohistochemical and Golgi staining

At P12 ( $n = 6$  per treatment group per sex) and P45 ± 5 ( $n = 8$  per treatment group per sex), mice were deeply anaesthetized via intraperitoneal administration of **pentobarbital** (Pentacour, 150 mg·kg<sup>-1</sup>). Animals at P45 were randomly selected from behavioural groups 30 min after completion of tests. The brains were removed from the skull, and the right or left hemisphere was selected randomly, immersed in 6% buffered formaldehyde (Histofix; Histolab products AB, Västra Frölunda, Sweden), and stored at 4°C until further processing. At the time of tissue processing, hemispheres were placed in a cryoprotective solution containing 30% (w·v<sup>-1</sup>) sucrose for 48 h followed by placement on copper blocks for freezing in cold isopentane (Sigma Aldrich). Free-floating 40-µm-thick brain sections were cut coronally on a cryostat (Leica, CM 3050 S, Germany) including the hippocampus (bregma –0.94 mm to –4.20 mm). The hippocampus was selected as structural abnormalities in this brain region have been observed in children with ASD (Chaddad et al., 2017; Schumann et al., 2004), and the hippocampus contains a high percentage of excitatory synapses (Megias et al., 2001). Five series of sections were collected based on a systematic sampling principle and a section-sampling fraction of 1/8 (Gundersen, 2002) by selecting the first section of each series randomly using a random table. Therefore, each series included 8–10 sections with a fixed distance of 320 µm (8 × 40 µm).

The contralateral hemisphere was processed for rapid Golgi-Cox staining for impregnation of individual pyramidal neurons in the hippocampus using the FD Rapid Golgi Stain TM Kit (FD Neuro Technologies, Inc., Columbia, MD) following the manufacturer's instructions as described previously (Treccani et al., 2019). Briefly, Golgi-stained hemispheres were sliced coronally (section thickness: 170 µm for P45 and 150 µm for P12) on a vibratome (Leica, VT1200S Semiautomatic Vibrating Blade Microtome, Wetzlar, Germany) and mounted on gelatin-coated slides.

Systematic sampling ensured that the distribution of left and right hemispheres was equal between the groups.

## 2.5 | Histological and immunohistochemical staining

The immuno-related procedures used comply with the recommendations made by the *British Journal of Pharmacology Guidelines*

(Alexander et al., 2018). One set of sections was Nissl stained with a 0.25% thionin solution (Sigma T3387) for determination of the volume of hippocampal subregions under light microscopy.

The rest of the series were labelled using primary antibodies for three-dimensional (3D) quantification of Reelin+ cells and 3D reconstruction of ionized calcium binding adaptor molecule 1 (Iba1) + microglia. Briefly, free-floating 40- $\mu$ m-thick sections were washed in phosphate-buffered saline (PBS, Gibco Invitrogen, Waltham, MA, USA) for 20 min. Sections were incubated in target retrieval solution (Dako, Glostrup, Denmark) at 85°C for 40 min for antigen retrieval. Afterwards, sections were washed for 20 min in PBS, followed by blocking of endogenous peroxidases (3% H<sub>2</sub>O<sub>2</sub> in PBS, Sigma Aldrich) for 10 min. Thereafter, sections were washed with PBS containing 0.02% Triton-X-100 (PBS-T, Sigma Aldrich) and then incubated with rabbit anti-Iba1 (1:1000, FUJIFILM Wako Shibayagi Cat# 01-1874, [RRID:AB\\_2314666](#)) and mouse monoclonal anti-reelin (1:1500, Abcam Cat# ab78540, [RRID:AB\\_1603148](#)) overnight at 4°C. The next day, sections were washed in PBS-T and subsequently incubated in polyclonal secondary biotinylated goat-anti-rabbit antibody (1:250, Vector Laboratories, Olean, NY, USA) in PBS-T for 2 h in room temperature (RT). Sections were washed in PBS-T followed by incubation in ABC elite solution (1.5% solution A + 1.5% solution B in PBS, Vector Laboratories) for 1 h at room temperature. Afterwards, sections were washed in PBS-T for 20 min, and immunolabelling was performed by using 3,3'-diaminobenzidine solution (Acros Organics, Geel, Belgium). Sections were washed in distilled water and stored in PBS. Finally, sections were mounted on gelatin-coated slides (1.3%, Sigma Aldrich), dehydrated through a graded series of alcohol (70%, 96%, and 99%), cleared in xylene for 10 min and coverslipped.

## 2.6 | Image acquisition of neurons, neuronal dendritic spine reconstruction and analysis

In Golgi-stained sections, six pyramidal neurons (six apical and six basal dendrites) per mouse were selected from the CA1 subregion for morphological analysis. The 3D capturing of neuronal images was performed using a light microscope modified for stereology with a digital camera (Leica DFC 295, Germany) and newCAST™ software (Visopharm, Hørsholm, Denmark). Pyramidal neurons were identified by their triangular-shaped soma from which apical dendrites and basal dendrites protrude. Selection criteria for sampling by the optical disector were as follows: (1) neurons were completely separated from other cells, (2) all dendrites were intact, and (3) the soma of the neuron was in the middle of the thickness of the section. Using a 63 $\times$  oil-immersed lens, z-stacks of images were captured with a z-plane step size of 1  $\mu$ m. The 3D analysis of reconstructed neurons including dendritic spines was performed using Filament Tracer algorithm of the Imaris software (version 8.4, Bitplane A.G., Zurich, Switzerland, [RRID:SCR\\_007370](#)) (Treccani et al., 2019). For 3D reconstruction, the longest diameter of the cell body was used as a starting point. Branch endpoints and bifurcations were then manually selected through which branches and dendrites were traced. Morphological neuronal

parameters were (1) apical/basal dendrite length, (2) number of apical/basal dendritic terminals, (3) convex hull volume, and (4) Sholl analysis to estimate the complexity of the dendritic arborization. The analysis performed was based on regularly spaced concentric circles centred on the neuronal soma. The sum of the number of intersecting dendrites for all circles was quantified for each neuron in intervals of 20  $\mu$ m (Sholl, 1953; Treccani et al., 2019).

In addition to the neuronal morphology, general morphological spine parameters were determined: (1) number of spines on apical/basal dendrites, (2) mean spine density (spines/10  $\mu$ m), (3) spine area, (4) spine length, (5) spine neck length, (6) spine diameter, and (7) spine neck diameter (Kim et al., 2013). Dendritic spines were also classified into three morphological subtypes using the automated Imaris spine classification analysis: (1) stubby spines with a length less than 1  $\mu$ m, lacking a spine head and with an apparent neck, (2) mushroom spines with a length less than 3  $\mu$ m and characterized by a short neck and large spine head, and (3) long-thin spines with mean width of head  $\geq$  mean width of neck and with elongated spine necks. General morphological parameters were calculated also for the different spine types.

## 2.7 | Image acquisition, 3D reconstruction, and analysis of microglia

Iba1 stains all microglia phenotypes. In order to determine morphological changes associated with activation of microglia (Boche et al., 2013; Kettenmann et al., 2011), we determined length and number of microglia processes as well as number of intersections on Iba1 stained sections. A total of 10 Iba1-positive microglia in the stratum radiatum (SR) of the hippocampal CA1 area were selected in each animal at P12 and P45 ( $n = 6$  per treatment group per sex) for 3D reconstruction and morphological analysis. Selection criteria for microglia were as follows: (1) cell bodies must be in the middle of the section thickness with a clear border, (2) all branches are intact, and (3) branches of the cell should be easily distinguishable from other cells or background staining. A systematic set of Z-stacks of images and z-plane step size of 1  $\mu$ m by selecting the middle of section as zero was obtained on Iba1 stained sections by using a 63 $\times$  oil-immersed lens on a light microscope modified for stereology. This acquisition procedure ensured capturing more than one microglia per image (Ardalan et al., 2017). The captured images were analysed using the Filament Tracers algorithm in the Imaris software. Morphological parameters were (1) number of the cellular branches, (2) total length of the branches, and (3) Sholl analysis based on the radial distance from the centre of the microglia soma in 5  $\mu$ m.

## 2.8 | Estimation of density of number of Iba1+ microglia

Unbiased density of Iba1+ microglia (including ramified and amoeboid) in the CA1 SR subregion of the hippocampus was quantified on

sections with section sampling fraction (SSF) (1/16) and area sampling fraction (ASF = 10%) using 63× oil-immersed lens and optical probe with the height of 20 μm. The density of cells was calculated according to the following formula (McNaught, 1997).

$$N = \Sigma Q^- / V$$

where  $N$  is the total number of microglia per volume of brain region;  $\Sigma Q^-$  is the number of counted microglia; and  $V$  is the volume of regions of interest per sampling frame.

## 2.9 | Estimation of total number of Reelin+ cells

At P12 and P45, unbiased counting of number of Reelin+ cells was performed in the CA1 subregion (including CA1 stratum oriens, CA1 pyramidal cells and CA1 stratum radiatum) of hippocampus using 63× oil-immersed objective lens and applying the optical fractionator method (Gundersen, 1986). Delineation of the CA1 area was based on differentiating the CA1 pyramidal cell layer from the CA2/CA3 pyramidal cell layer (subregion with larger dense packed cells compared with CA1) and the subiculum (area with smaller cell number density and bigger pyramidal cell size compared with pyramidal cells found in CA1) with a 5× objective lens. To eliminate the effect of shrinkage of tissue sections due to tissue preparation, the optimal disector height was calculated from a pilot study where cells were counted through the full thickness of eight selected hippocampal sections (systematic random sampling of sections between animals). The z-position of each counted Reelin+ cell and the section thickness per sampling frame were measured. z-plot (histogram) of the counted cells indicates constant cell density in the thickness from 5 μm to 25 μm which corresponds to full penetration and linear shrinkage of the section in the thickness of 20 μm. The criterion for counting was that the cell soma was in focus and fully or partially in the unbiased counting frame without touching the forbidden lines. The following formula was used to calculate the total number of cells (Ardalan et al., 2016):

$$N = \frac{1}{SSF} \cdot \frac{1}{ASF} \cdot \frac{1}{HSF} \cdot \Sigma Q^-$$

where  $N$  is the total number of Reelin+ neurons in CA1 area;  $\Sigma Q^-$  is the number of counted cells;  $SSF$  is the section sampling fraction (1/8);  $ASF$  is an area sampling fraction; and  $HSF$  is the height sampling fraction (mean of the  $Q^-$ -weighted height of the disector).

## 2.10 | Morphological analysis of Reelin+ cells

Reelin+ cells can be divided into subgroups based on cell size (small vs. large soma-dendritic-axonal arborizations) (Pelkey et al., 2017). Therefore, we measured the Reelin+ cell soma in the CA1 subregion of hippocampus at P12 and P45 by applying spatial rotator estimator

independent of tissue orientation (Rasmusson et al., 2013). The cell volume estimation was performed with a 100× oil-immersion objective lens by using a virtual 3D probe and making six intersection points between cell boundaries and test rays in a series of parallel focal planes with a good resolution. We sampled randomly 50–80 cells per animal by the optical disector with a height of 20 μm with the area sampling fraction (ASF = 1%).

## 2.11 | Quantification of hippocampal subregion volumes on histological sections

The volume of the whole hippocampus and hippocampal subfields (granular cell layer [GCL] and CA1 striatum radiatum [CA1 SR]) were estimated on Nissl-stained sections by using the unbiased Cavalieri estimator (Gundersen et al., 1988) using a 10× objective lens under light microscope. Of note, volume measurement of hippocampal subregions on the cryostat sections has the advantages of the negligible amount of shrinkage in the x- and y-axes. The formula used for determining the volume of the subregions was

$$V = \Sigma P \cdot \left( \frac{a}{p} \right) \cdot T \cdot \frac{1}{SSF}$$

where  $\Sigma P$  is the total number of the points hitting the region of interest per animal,  $(a/p)$  is the area per test point,  $T$  is the section thickness (40 μm), and  $SSF$  is the section sampling fraction (1/8).

## 2.12 | Magnetic resonance imaging

### 2.12.1 | Sample preparation

Mice at P45 ( $n = 5$  per treatment group per sex) were deeply anaesthetized via intraperitoneal administration of (Pentacour, 60 mg·ml<sup>-1</sup>), perfusion-fixed with heparin (10 U·ml<sup>-1</sup>)-treated 0.9% saline (pH = 7.3) for 2 min, followed by ice-cold 6% buffered formaldehyde (pH = 7.2–7.4) for 2 min. Following fixation, the head was separated from the body just below the skull base. The skin was then removed from the head to avoid susceptibility artefacts in the MRI due to air bubbles trapped in the fur during imaging. This in-skull brain preparation was previously used (Qvist et al., 2018) and has the advantage of avoiding deformation of the brain.

### 2.12.2 | Data collection

MRI was performed using a 9.4T preclinical MRI system equipped with a bore-mounted 25-mm quadrature coil used for both excitation and reception. Prior to imaging, samples were washed for at least 24 h in phosphate buffered saline (PBS, Sigma USA, P4417-50TAB) to increase signal by removal of excess fixative. The sample was then securely placed in a tube filled with

fluorinert (FC-770, 3M inc.), which was fitted into the coil in such a manner that all sample vibration was avoided. High resolution B0-mapping was employed to ensure good shim conditions (particularly important for the diffusion kurtosis imaging (DKI) data collection).

Volumetric data were acquired at an in-plane resolution of  $64 \mu\text{m} \times 64 \mu\text{m}$  and a slice thickness of  $200 \mu\text{m}$  using a rapid Imaging with refocused echoes (RARE) sequence. Scan details were effective echo time,  $TE = 10 \text{ ms}$ , repetition time ( $TR = 3133 \text{ ms}$ ), 4 averages, RARE factor = 2. Total scan time was 23 min. After acquisition, data were inspected for artefacts and exported in the dicom format for volumetric processing. DKI data were acquired at  $200\text{-}\mu\text{m}$  isotropic resolution using a segmented diffusion weighted echo planar imaging (EPI) sequence. Five unweighted images were acquired in each slice for normalization along with 20 encoding directions at each of four b-values (0, 0.8, 1.8, and  $2.0 \text{ ms}\cdot\mu\text{m}^{-2}$ ). Diffusion timings were  $\delta/\Delta = 7/16 \text{ ms}$ , and remaining parameters were 5 avs,  $TE = 30.27 \text{ ms}$ ,  $TR = 3000 \text{ ms}$ ,  $BW = 277 \text{ kHz}$ , 80 axial slices.

### 2.12.3 | DKI analysis

DKI is an advanced neuroimaging modality which is an extension of diffusion tensor imaging by estimating the kurtosis (skewed distribution) of water diffusion based on a probability distribution function. DKI data was imported in Matlab (Mathworks Inc, USA) and preprocessed as described previously. Briefly, data were Rician noise floor adjusted (Hansen et al., 2013), denoised, and corrected for Gibbs-ringing (Hansen et al., 2017). Following a normalization step, the data were fitted to the DKI signal equation using non-linear optimization (Matlab, The Mathworks, USA) as in Hansen et al. (2013). From the DKI fit, the mean diffusivity (MD) and mean kurtosis (MK) were calculated for each sample (Hansen et al., 2017; Jensen et al., 2005). Hippocampus was then delineated on the unweighted diffusion images for each sample. These delineations were used to extract average hippocampal MD and MK values for each sample. At this point, blinding was lifted, and the groups were tested for statistical differences in MD and MK using Matlab's two-sample Kolmogorov–Smirnov test.

### 2.12.4 | Volumetric analysis from MRI images

The whole brain and hippocampi were delineated in the RARE MRI data using ITK-snap (RRID:SCR\_002010) (Yushkevich et al., 2006). From these delineations, the brain and hippocampi volumes were calculated as the product of the total brain and total hippocampal voxel count and the nominal MRI voxel volume.

## 2.13 | Quantitative reverse transcription PCR

At P12 and P45 ( $n = 10$  per treatment group per sex), mice were deeply anaesthetized via intraperitoneal administration of

pentobarbital (Pentacour), and the right and left hippocampi were rapidly dissected and stored at  $-80^\circ\text{C}$  until analysis. Total mRNA was isolated from the hippocampus using the miRNeasy mini kit (Qiagen Inc.) according to the manufacturer's recommendations. Total RNA concentration and purity were measured by a Nanodrop (Thermo Scientific) at 235, 260, and 280 nm. cDNA was prepared from  $1 \mu\text{g}$  RNA in a  $20\text{-}\mu\text{l}$  reaction using QuantiTect Reverse Transcription Kit (Qiagen). Each PCR ( $20 \mu\text{l}$ ), contained  $2\text{-}\mu\text{l}$  cDNA ( $12 \text{ ng}$ ),  $10\text{-}\mu\text{l}$  QuantiFast SYBR Green PCR Master Mix (Qiagen), and  $2\text{-}\mu\text{l}$  PCR primer (QuantiTect Primer Assay, Qiagen), were run on a LightCycler 480 (Roche, Sweden). The following primers were used Nlgn1 QuantiTect Primer Assay (QT00167580), Nrnx3 QuantiTect Primer Assay (QT00166621), and Pvr11 (nectin-1) QuantiTect Primer Assay (QT00171703) all from Qiagen. Melting curve analysis was performed to ensure that only one PCR product was obtained. For quantification and for estimation amplification efficiency, a standard curve was generated using increasing concentrations of cDNA. The amplified transcripts were quantified with the relative standard curve and normalized by the cDNA concentration using the Quant-IT OliGreen ssDNA Assay kit (Fisher Scientific).

## 2.14 | Statistical analysis

All data were analysed using SPSS (IBM Corp. Released 2013, Version 24.0. Armonk, NY, USA, RRID:SCR\_002865). Graphs were created using Prism 8 (GraphPad Software Inc., USA, RRID:SCR\_002798). Prior to statistical tests, normal distribution of data was checked by making a Q–Q plot of the data. The variance homogeneity of data was also examined by Levene's test. If the distribution of data was not normal, a logarithmic transformation was employed before statistical testing. For the three-chamber test, repeated measures analysis of variance (ANOVA) was used to compare time spent in the chamber containing the stimulus mouse and time spent in the chamber containing the empty pencil cup. Continuous morphological, molecular data and sociability index were compared using two-way ANOVA followed by Tukey's post hoc test (equal variances) and Games-Howel (not equal variances) with adjusted  $p$  values. DKI data analysis was performed in MATLAB (Mathworks Inc, USA), as described previously (Hansen et al., 2017). The data was fitted to the DKI signal equation using non-linear optimization (MATLAB, The MathWorks, USA). From the DKI fit, the average HC MD and MK were calculated for each sample. At this point, blinding was lifted, and the groups were tested for statistical differences in HC MD and MK.  $P \leq 0.05$  was considered as significantly different distributions using Matlab's Two-sample Kolmogorov–Smirnov goodness-of-fit hypothesis test. This tests if independent random samples,  $X_1$  and  $X_2$ , are drawn from the same underlying continuous population. The mean values from six neurons and 10 microglia of each animal in the morphological studies were treated as a single measurement in the data analysis. Statistical analysis was undertaken only for studies where each group size was at least  $n = 5$ . No data with less than  $n = 5$  were included, and there were no data points excluded in the study. In all statistical analysis, the group

size was used as the number of independent values (i.e., technical replicates were not used as independent values). The sample size was calculated based on the previous published studies which applied the same methods of quantifications (Ardalan et al., 2017; Treccani et al., 2019). In multigroup studies with parametric variables, post hoc tests were run only if  $F$  achieved  $P \leq 0.05$ . In all cases, the significance level was assumed at  $P \leq 0.05$ . The results are presented as mean  $\pm$  standard deviation. Partial  $\eta^2$  for the effect size of LPS treatment and sex on the quantified variables was calculated by considering observed power using  $\alpha = 0.05$  based on the following formula:

$$\eta^2 = \frac{SS_{\text{between}}}{SS_{\text{total}}}$$

where  $SS$  = sum of squares

## 2.15 | Nomenclature of targets and ligands

Key protein targets and ligands in this article are hyperlinked to corresponding entries in <http://www.guidetopharmacology.org>, and are permanently archived in the Concise Guide to PHARMACOLOGY 2021/22 (Alexander, Christopoulos et al., 2021; Alexander, Fabbro et al., 2021).

## 3 | RESULTS

### 3.1 | PIA induces brain overgrowth and impairs fibre integrity in male adolescent mice

A feature in children with autism is increased brain volumes (Sparks et al., 2002). As such, we performed volume measurements of the whole brain (excluding olfactory bulb and cerebellum) (Figure 1a,b) and entire hippocampi (Figure 1d,e) from MRI images at P45. The MRI analysis of brain volume revealed significant main effect of sex with significant LPS  $\times$  sex interaction, ( $F_{(1,19)} = 23.420$ ,  $P \leq 0.05$ ;  $F_{(1,19)} = 8.474$ ,  $P \leq 0.05$ , respectively). Games-Howell post hoc analysis revealed that LPS significantly increased the volume of brain in male mice ( $P \leq 0.05$ ) without significant effect in female mice ( $P > 0.05$ , Figure 1c). Moreover, the MRI analysis showed significant main effect of sex and interaction with LPS treatment on the volume of hippocampi in males ( $F_{(1,19)} = 4.855$ ,  $P \leq 0.05$ ;  $F_{(1,19)} = 7.769$ ,  $P \leq 0.05$ ). Tukey post hoc analysis revealed a significantly larger size of hippocampi in male LPS group compared with male saline mice ( $P \leq 0.05$ ) without significant effect in female LPS mice ( $P > 0.05$ , Figure 1f). Partial  $\eta^2$  for the effect of sex and treatment on the whole brain volume were 0.59 and 0.09 which indicated large and moderate effects of sex and LPS treatment, while partial  $\eta^2$  for the effect of sex and treatment on the hippocampi volume were 0.23 and 0.19, indicating large effects of both sex and LPS treatment on the hippocampi volume.

The volume measurement of hippocampal subregions on Nissl stained sections (Figure 1g) showed significant main effects of sex and LPS treatment on the volume of the CA1 SR subregion of hippocampus,

respectively ( $F_{(1,29)} = 26.335$ ,  $P \leq 0.05$ ;  $F_{(1,29)} = 19.035$ ,  $P \leq 0.05$ ) without significant effect on the volume of GCL area (Figure 1h). Tukey post hoc analysis indicated that the volume of the CA1 SR area was significantly larger in male LPS mice versus male saline group ( $P \leq 0.05$ ) without significant changes in female LPS group ( $P > 0.05$ , Figure 1i). Partial  $\eta^2$  for the effect of sex and LPS treatment were 0.50 and 0.42 which indicated large effect of sex and LPS treatment on the volume of CA1 SR area. Based on these findings, all further morphological analyses were performed in the CA1 SR region of the hippocampus.

DKI, an emerging increasingly used technique that provides complementary information to traditional diffusion techniques on the complexity of the microstructure (Hansen, 2020), revealed a shift towards higher MD values in dorsal and ventral hippocampus in adolescent males after LPS as seen in the MD probability distributions (Figure 2a,b). In contrast, MD values were lower in female LPS mice compared with saline female animals (Figure 2a,c). There were no significant changes in MK in either males or females after LPS ( $P > 0.05$ , Figure 2d,e) although a tendency to lower MK values was seen in all LPS animals.

### 3.2 | PIA alters microglia response at P12 and P45

To determine the microglia response following PIA connected with autism, we determined the density of microglia cells and performed a detailed analysis of 3D branching pattern in reconstructed Iba1 + cells in the CA1 SR subregion of the hippocampus in saline (Figure 3d) and LPS (Figure 3h) treated mice.

At P12, there was a significant effect of LPS  $\times$  sex on the length and number of microglia processes ( $F_{(1,20)} = 8.368$ ,  $P \leq 0.05$ ;  $F_{(1,20)} = 6.048$ ,  $P \leq 0.05$ , respectively), with the main effects of sex ( $F_{(1,20)} = 5.841$ ,  $P \leq 0.05$ ;  $F_{(1,20)} = 9.736$ ,  $P \leq 0.05$ ) and LPS treatment ( $F_{(1,20)} = 51.815$ ,  $P \leq 0.05$ ;  $F_{(1,20)} = 42.105$ ,  $P \leq 0.05$ ). At baseline, the microglia processes were significantly shorter and with fewer number of processes in female saline compared with the male saline groups ( $P \leq 0.05$ , Figure S1A,B). Microglia processes were significantly shorter and fewer in male LPS compared with male saline mice ( $P \leq 0.05$ ) and in female LPS compared with saline female group ( $P \leq 0.05$ , Figure S1A,B). Moreover, Sholl analysis showed that the number of process intersections at 10–40  $\mu\text{m}$  away from the cell soma were significantly lower in male LPS mice than male saline group ( $P \leq 0.05$ ), while in female mice, the complexity of microglia processes was only affected by LPS, 20  $\mu\text{m}$  away from cell soma ( $P \leq 0.05$ , Figure S1C).

At P45, there were significant main effects of sex ( $F_{(1,20)} = 5.969$ ,  $P \leq 0.05$ ) and LPS treatment ( $F_{(1,20)} = 63.534$ ,  $P \leq 0.05$ ) with the partial  $\eta^2$  of 0.23 and 0.76 on the length of microglia processes, and a significant effect of LPS treatment on number of microglia branches ( $F_{(1,20)} = 45.518$ ,  $P \leq 0.05$ ), with the  $\eta^2$  of 0.69, was observed (Figure 3a,b). At baseline, the length and number of microglia processes were not different between male and female saline groups ( $P > 0.05$ , Figure 3a,b). Sholl analysis showed that the complexity of microglia processes (intersections at 5–45  $\mu\text{m}$  away from the cell soma) in male LPS mice was significantly lower compared with the male saline group

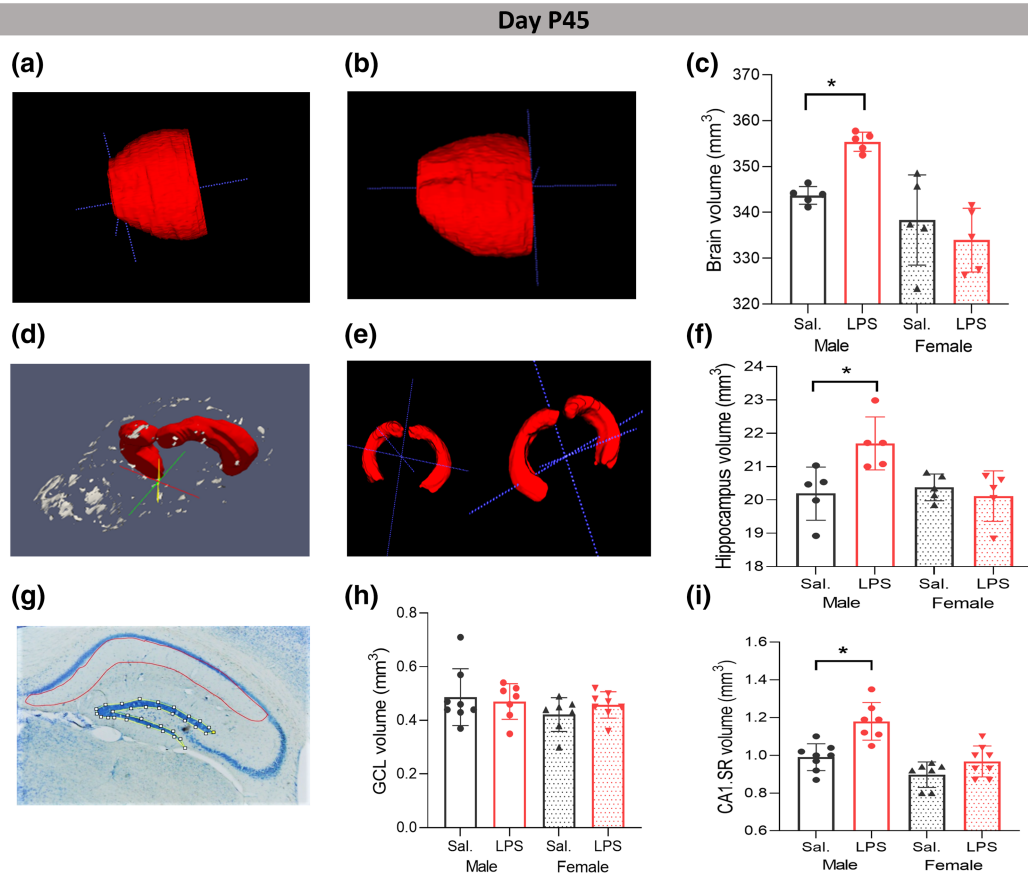


**FIGURE 1** Effects of postnatal immune activation (PIA) on brain, hippocampi, and hippocampal subregion volumes at P45. Examples of measured volumes of the whole brain (excluding olfactory bulb and cerebellum) in male saline (Sal) (a), male LPS (b), and of hippocampi (d), in male saline (e, left) and male LPS (e, right), on MRI images at P45. There were significant differences in the volume of whole brain and hippocampi between male saline and male LPS groups (c, f) ( $N = 5$  per group). Examples of delineated granular cell layer (GCL) (yellow) and CA1 striatum radiatum (CA1 SR) (red) (g) on Nissl-stained sections at P45. Volume measurement of GCL (h) and CA1 SR (i) subregions ( $N = 8$  per group). Ex vivo images were generated using ITK-snap and ParaView-5.8.0-RC1-Windows-Python3.7 software (Ayachit, Utmarsh, *The ParaView Guide: A Parallel Visualization Application*, Kitware, 2015, ISBN 978-1930934306). Two-way ANOVA with Games-Howell and Tukey post hoc tests were used for the statistical analysis. \* $P \leq 0.05$

( $P \leq 0.05$ ), while in LPS compared with saline female mice, the complexity of microglia processes was affected at 10–30  $\mu\text{m}$  away from cell soma ( $P \leq 0.05$ , Figure 3c). Representative figures of Iba1<sup>+</sup> stained sections in male saline (Figure 3f) and male LPS (Figure 3g). There were significant main effects of LPS  $\times$  sex ( $F_{(1,20)} = 6.240$ ,  $P \leq 0.05$ ), sex ( $F_{(1,20)} = 12.589$ ,  $P \leq 0.05$ ) and LPS treatment ( $F_{(1,20)} = 14.057$ ,  $P \leq 0.05$ ) with the partial  $\eta^2$  of 0.38 and 0.41 on the density of microglia in the CA1 SR subregion of the hippocampus. Games-Howell post hoc analysis indicated significantly higher density of microglia in male LPS group compared with saline treated mice ( $P \leq 0.05$ ) without significant changes in the female mice ( $P > 0.05$ ) (Figure 3h).

### 3.3 | Sex-specific difference in autistic behavioural phenotypes following PIA

Repetitive behaviour and impairment in sociability are core symptoms of autism. The marble burying test showed a significant main effect of

LPS ( $F_{(1,39)} = 41.25$ ,  $P \leq 0.05$ ) and post hoc analysis revealed that male and female offspring displayed increased repetitive behaviour after LPS exposure ( $P \leq 0.05$ , Figure 4a). No significant difference between male and female saline groups was observed ( $P > 0.05$ ). Partial  $\eta^2$  for the effect treatment was 0.53, which indicated a large effect of LPS treatment on the number of buried marbles as a measure of repetitive behaviour.

In the three-chamber social interaction test, comparison between time spent in the chamber containing the stimulus (novel) mouse and time spent in the chamber containing the empty pencil cup showed that male saline mice spent significantly more time in the stimulus mouse chamber ( $P \leq 0.05$ ), while male LPS group showed significant less time spent in the novel mouse chamber ( $P \leq 0.05$ , Figure 4b). In females, there was no preference to any of the two chambers ( $P > 0.05$ , Figure 4b). The results showed a significant main effect of LPS on sociability index (SI) with significant LPS  $\times$  sex interaction, respectively ( $F_{(1,39)} = 11.55$ ,  $P \leq 0.05$ ;  $F_{(1,39)} = 7.33$ ,  $P \leq 0.05$ ), and post hoc analysis revealed that LPS reduced SI only in male offspring

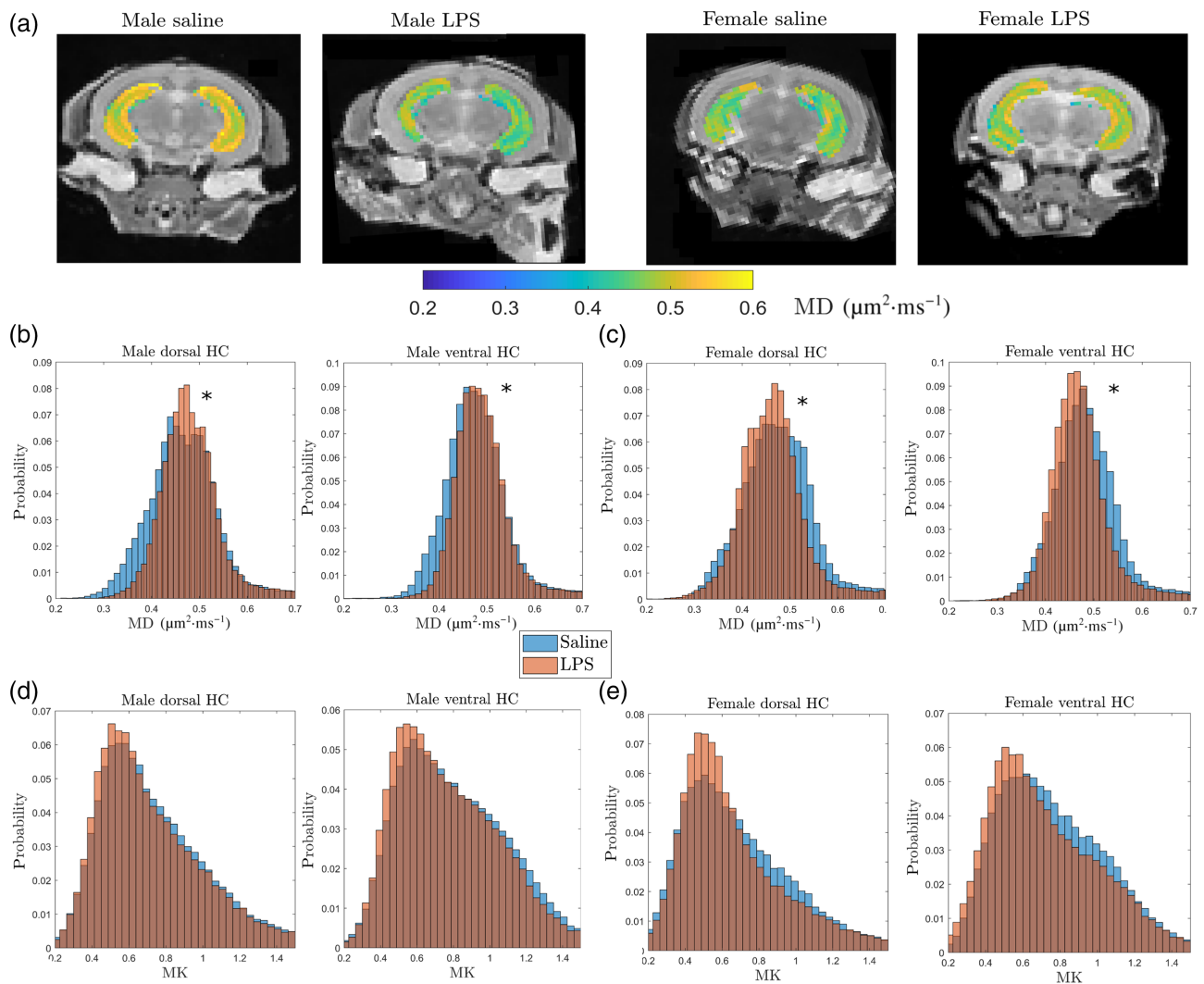


**FIGURE 2** Effects of postnatal immune activation (PIA) on MRI kurtosis of hippocampi at P45. Mean diffusivity (MD) and mean kurtosis (MK) measurements were acquired from MRI images at P45 in male and female mice following PIA. Example showing MD images in groups at the hippocampal level (a). Histograms showing that the distribution of MD in dorsal and ventral hippocampus in PIA males (brown) was increased compared with saline males (blue) (b), while MD was decreased in PIA females (brown) compared with saline females (blue) (c). There were no changes in mean kurtosis (MK) in dorsal or ventral hippocampus in males (d) and females (e) in saline (blue) and LPS (brown) treated animals ( $N = 5$  per group). MD reflects overall water mobility (averaged over all directions) and is given in units of  $\mu\text{m}^2\cdot\text{ms}^{-1}$ . In the histogram, \* indicates significantly different distributions at the  $P \leq 0.05$  level using Matlab's two-sample Kolmogorov–Smirnov goodness-of-fit hypothesis test. This tests if independent random samples,  $X_1$  and  $X_2$ , are drawn from the same underlying continuous population

( $P \leq 0.05$ , Figure 4c). No effect of sex or LPS exposure on the time spent in the middle chamber was observed (Figure 4d). However, we found a significant difference in time spent exploring (sniffing time) the stimulus mouse cup compared with the empty cup in all groups ( $P \leq 0.05$ ), except male LPS ( $P > 0.05$ , Figure 4e).

Regarding locomotor activity, we did not find differences in the number of times crossing the chambers between the groups ( $P > 0.05$ ) (Figure 4f).

Self-grooming was increased in LPS injected mice compared with the saline animals without sex-dependent effects ( $P \leq 0.05$ ) (Figure 4g).

### 3.4 | PIA does not affect branching patterns of neuronal apical or basal dendrites

At P12, we found no effect of sex and LPS treatment on the length ( $F_{(1,28)} = 0.514$ ,  $P > 0.05$ ;  $F_{(1,28)} = 0.275$ ,  $P > 0.05$ ) and number of the apical dendrites branches ( $F_{(1,28)} = 0.127$ ,  $P > 0.05$ ;  $F_{(1,28)} = 0.254$ ,  $P > 0.05$ ). Neither did Sholl analysis reveal any effects on the branching patterns of apical dendrites ( $P > 0.05$ ). Similarly, no significant differences in the length, number, and complexity of basal dendrites were observed between LPS and saline injected mice ( $P > 0.05$ , Figure S2).

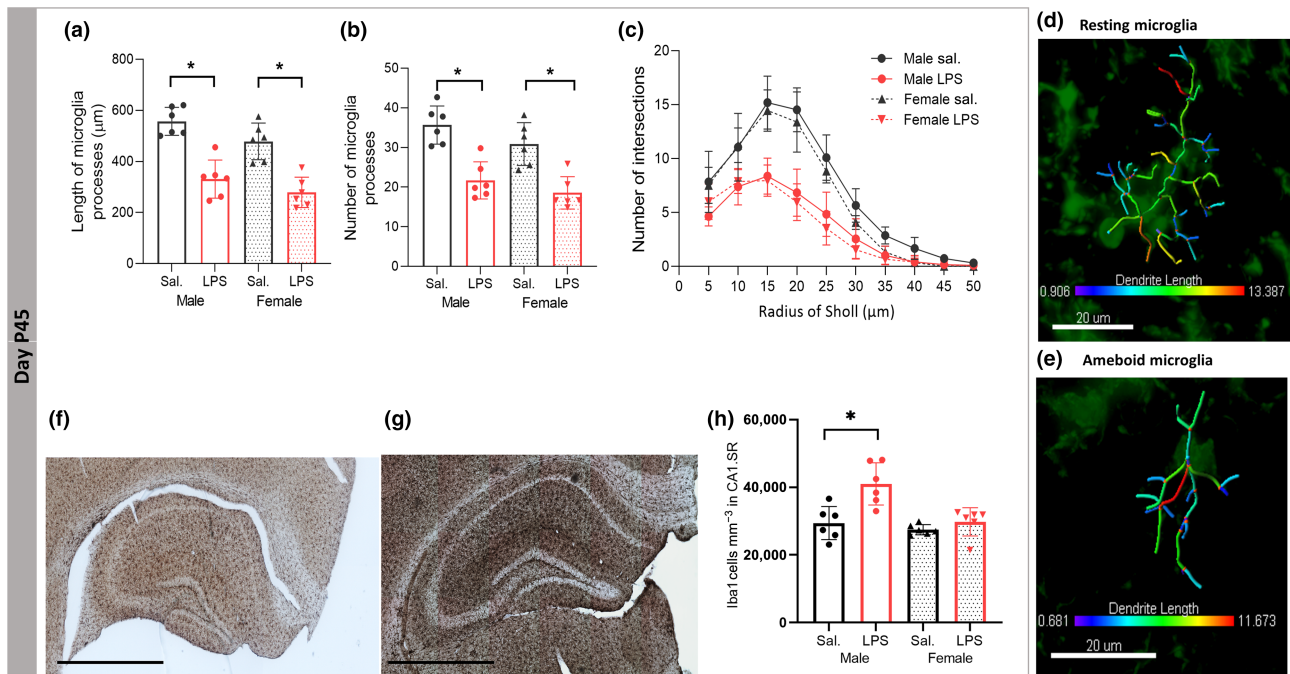


**FIGURE 3** Effects of postnatal immune activation (PIA) on microglia morphology and number at P45. Microglia were identified by Iba-1 immunohistochemistry in the hippocampus at P45. Microglia morphology analysis showed shorter process lengths and smaller number of processes in the CA1 SR subregion of the hippocampus in male and female PIA animals compared with saline (Sal) groups at P45 (a, b). Branching pattern analysis of microglia demonstrated that the number of branching intersections at various distances away from the cell soma was significantly lower in the LPS group versus the saline group at P45 (c), independent of sex. Examples of 3-D reconstructed microglia in the CA1 SR subregion of hippocampus in male saline mouse (d) and male LPS mouse (e); representative images of Iba1 hippocampal stained sections in male saline (f) and male LPS (g). Significant effect of PIA on microgliosis in CA1 SR subregion of hippocampus in male LPS mice (h) ( $N = 6$  per group). Scale bar is 800  $\mu\text{m}$ . Two-way ANOVA with a Tukey post hoc test was used for the statistical analysis.  $*P \leq 0.05$

At P45, we found no effect of sex and LPS treatment on the length and number of branches on apical dendrites or basal dendrites. Moreover, Sholl analysis revealed that the branching patterns of apical dendrite ( $P > 0.05$ ) or basal dendrites ( $P > 0.05$ ) were not different between the groups (Figure S3).

### 3.5 | PIA increases convex hull volume of neuronal apical dendrites in males

To determine the size of the dendritic field, we measured the convex hull volume of apical and basal dendrites. There was a significant sex  $\times$  LPS interaction effect on convex hull volume of apical dendrites ( $F_{(1,20)} = 15.468$ ,  $P \leq 0.05$ ) with the significant main effects of sex and LPS ( $F_{(1,20)} = 14.689$ ,  $P \leq 0.05$ ;  $F_{(1,20)} = 4.506$ ,  $P \leq 0.05$ ) and partial  $\eta^2$  of 0.42 and 0.18, respectively. Tukey post hoc analysis demonstrated a significant increase of LPS treatment on convex hull volume of apical dendrites in male mice ( $P \leq 0.05$ ) with no LPS treatment effect in females ( $P > 0.05$ ) (Figure S4A). Example of 3D reconstructed apical dendrite convex hull from the CA1 subregion of the hippocampus is shown in male saline and male LPS mice (Figure S4B, C). At the level of basal dendrites, no significant difference in the convex hull volume of dendrites was observed between LPS and saline injected mice at P45 ( $P > 0.05$ , data not shown).

### 3.6 | PIA alters neuronal spine density in a sex-dependent manner

Neuronal spine density was determined on Golgi-stained sections on apical (Figure 5a) and basal (Figure 5b) dendrites. At P12, we found significant main effect of LPS treatment ( $F_{(1,28)} = 20.242$ ,  $P \leq 0.05$ ) on the spine density on apical dendrites, with the partial  $\eta^2$  of 0.41. Tukey post hoc analysis indicated a significant effect of LPS in male mice ( $P \leq 0.05$ ) with no significant LPS treatment effect in females ( $P > 0.05$ , Figure 5c).

There was a significant main effect of LPS treatment ( $F_{(1,28)} = 4.518$ ,  $P \leq 0.05$ ) on the spine density on basal dendrites with the partial  $\eta^2$  of 0.13. Tukey post hoc analysis indicated a significant increase of the spine density on basal dendrites in female mice ( $P \leq 0.05$ ) with no significant LPS treatment effect in males ( $P > 0.05$ , Figure 5d).

At P45, we found significant main effect of LPS injection ( $F_{(1,20)} = 4.653$ ,  $P \leq 0.05$ ,  $P \leq 0.05$ ) with the partial  $\eta^2$  of 0.18 on the spine density of apical dendrites, which indicated significant difference in the spine density between male saline and male LPS injected mice ( $P \leq 0.05$ ), while there was no difference in spine density between female saline and female LPS groups ( $P > 0.05$ , Figure 5e). There were no effects of sex and LPS treatment on spine density on basal dendrites (Figure 5f).

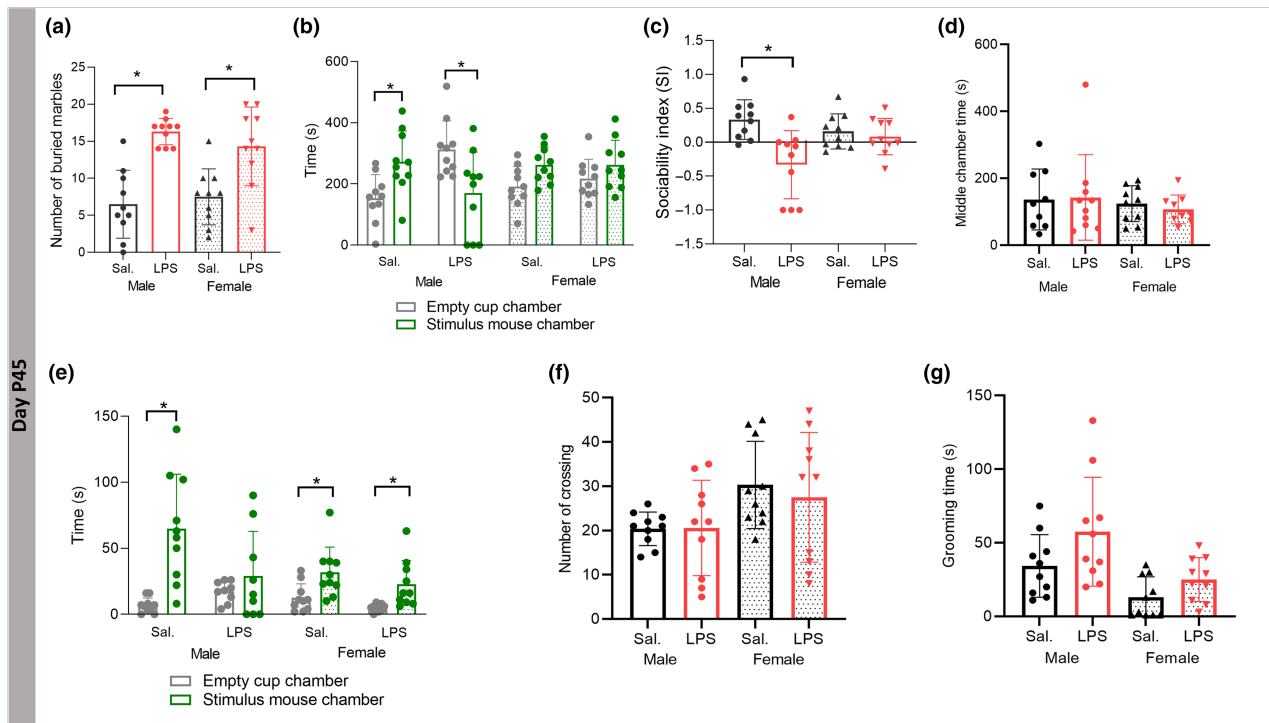


**FIGURE 4** Effects of postnatal immune activation (PIA) on autistic-like behaviours at P45. Stereotypic and repetitive behaviour was investigated by the marble burying test (a) and sociability by the three-chamber test (b, c) at P45. The marble burying test showed a significantly higher number of buried marbles in male and female LPS mice compared with saline (Sal) groups (a). There were significant main effects of LPS treatment on sociability (b) and social index (c) in male mice only. There was no difference in the time spent in the middle chamber between groups (d). Time spent exploring the cup with stimulus mice was significantly increased compared with the time spent exploring the empty pencil cup in male saline, female saline and female LPS groups, but not in the male LPS group (e). There was no difference in the number of chamber crossings (f) or time spent grooming (g) between any of the groups ( $N = 10$  per group). Two-way ANOVA with a Tukey post hoc test was used for the statistical analysis of marble test, sociability index (SI), middle chamber time, number of crossing, and grooming time; repeated measure ANOVA was used for the statistical analysis of chamber and sniffing times.  $*P \leq 0.05$

There was a significant negative correlation between the time spent in stimulus mouse chamber and the spine density on apical dendrites ( $r = -0.6$ ,  $P \leq 0.05$ ) (Figure S5A).

### 3.7 | PIA remodels neuronal spine morphology in a sex-dependent manner

Spine morphology is a crucial determinant of structural stability and function, so we next investigated effects of PIA on spine morphology. At P12, we found significant main effect of LPS treatment on apical dendrite spine area, spine length, spine diameter and spine neck length ( $F_{(1,28)} = 18.896$ ,  $P \leq 0.05$ ;  $F_{(1,28)} = 18.760$ ,  $P \leq 0.05$ ;  $F_{(1,28)} = 20.127$ ,  $P \leq 0.05$ ;  $F_{(1,28)} = 19.752$ ,  $P \leq 0.05$ ) with partial  $\eta^2$  of 0.40, 0.41, 0.41, and 0.43, respectively. Games-Howell post hoc analysis showed a significant increase after LPS on the spine area (Figure 6a), spine length (Figure 6b), spine diameter (Figure 6c), and spine neck length (Figure 6d) in male mice ( $P \leq 0.05$ ), without effect in female mice ( $P > 0.05$ ). At P45, there was a significant main effect of sex and sex  $\times$  LPS treatment interaction on the spine area ( $F_{(1,20)} = 6.935$ ,  $P \leq 0.05$ ;  $F_{(1,20)} = 11.987$ ,  $P \leq 0.05$ ) with the partial  $\eta^2$  of 0.25, spine

length ( $F_{(1,20)} = 5.274$ ,  $P \leq 0.05$ ;  $F_{(1,20)} = 18.166$ ,  $P \leq 0.05$ ) with the partial  $\eta^2$  of 0.20, spine diameter ( $F_{(1,20)} = 5.283$ ,  $P \leq 0.05$ ;  $F_{(1,20)} = 15.764$ ,  $P \leq 0.05$ ) with the partial  $\eta^2$  of 0.20 and sex  $\times$  LPS treatment interaction effect on the spine neck length ( $F_{(1,20)} = 14.847$ ,  $P \leq 0.05$ ). Tukey post hoc analysis demonstrated a significant effect of LPS treatment on spine area (Figure 6e), spine length (Figure 6f), spine diameter (Figure 6g), and spine neck length (Figure 6h) in male mice ( $P \leq 0.05$ ) without effects in female mice ( $P > 0.05$ ).

On basal dendrites at P12, our results indicated significant main effect of LPS treatment on the spine area, spine length, spine diameter, spine neck length, and spine neck diameter ( $F_{(1,28)} = 10.339$ ,  $P \leq 0.05$ ;  $F_{(1,28)} = 9.702$ ,  $P \leq 0.05$ ;  $F_{(1,28)} = 10.122$ ,  $P \leq 0.05$ ;  $F_{(1,28)} = 6.891$ ,  $P \leq 0.05$ ;  $F_{(1,28)} = 6.444$ ,  $P \leq 0.05$ ) with partial  $\eta^2$  of 0.27, 0.25, 0.26, 0.19, and 0.19, respectively. Tukey post hoc analysis indicated a significant effect of perinatal LPS treatment on the spine area, spine length, spine diameter, and spine neck length in the female mice ( $P \leq 0.05$ ) without effect in male mice ( $P > 0.05$ ) (Figure S6). Moreover, on basal dendrites at P45, our results indicated no effect of sex and LPS treatment on the spine area, spine length, spine diameter, and spine neck length of basal dendrites 40 days after LPS injection (Figure S7).

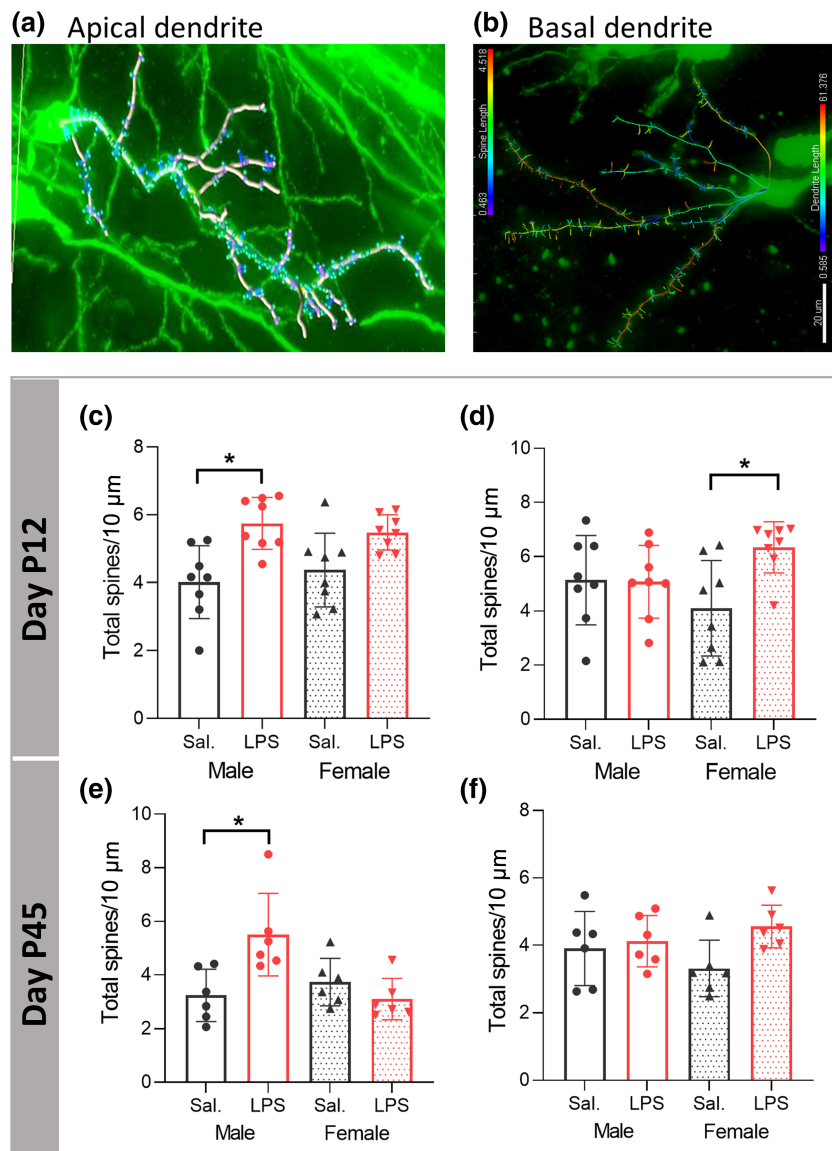


**FIGURE 5** Postnatal immune activation (PIA) alters neuronal spine density of pyramidal neurons in the CA1 area of hippocampus in a time- and sex-dependent manner. Analysis of spines on 3D reconstructed apical (a) and basal (b) dendrites was investigated on Golgi-Cox impregnated pyramidal neurons in the CA1 subregion of hippocampus in mice at P12 (c, d) ( $N = 8/\text{group}$ ) and P45 ( $N = 6$  per group) (e, f). The spine density on apical dendrites was significantly increased 1 week (c) and 40 days (e) after LPS injection in male mice compared to saline (Sal) injected mice. The spine density on basal dendrites was significantly increased 1 week (d) after LPS injection in female mice without significant changes at P45 (f). Two-way ANOVA with a Tukey post hoc test was used for the statistical analysis.  $*P \leq 0.05$

We found a significant negative correlation between time spent in the stimulus chamber and the spine neck length on apical dendrites ( $r = -0.477$ ,  $P \leq 0.05$ ) (Figure S7D); the neck length of both thin and mushroom spines ( $r = -0.465$ ,  $P \leq .05$ ;  $r = -0.528$ ,  $P \leq 0.05$ ) (Figure S5E,F).

### 3.8 | PIA alters density of different types of neuronal spines in a sex-dependent manner

To examine the effect of PIA on density of functionally different classes of spines, we analysed mushroom (mature), stubby (immature), and long-thin (immature) spines separately (Figure 7a). On apical dendrites at P12, two-way ANOVA showed no significant effect of sex and LPS treatment on the density of stubby spines ( $F_{(1,28)} = 1.148$ ,  $P > 0.05$ ;  $F_{(1,28)} = 1.437$ ,  $P > 0.05$ , Figure 7b), while there were significant effects of LPS on the density of mushroom spines ( $F_{(1,28)} = 12.788$ ,  $P \leq 0.05$ ), with the partial  $\eta^2$  of 0.31, and on the

density of long-thin spines ( $F_{(1,28)} = 25.119$ ,  $P \leq 0.05$ ), with the partial  $\eta^2$  of 0.47. The density of long-thin spines was increased in LPS males and females compared with respective saline group ( $P \leq 0.05$ , Figure 7c), while density of mushroom spines was significantly increased only in male mice after LPS ( $P \leq 0.05$ , Figure 7d). There were no effects of LPS on the density of different types of spines on basal dendrites (data not shown).

On apical dendrites at P45, two-way ANOVA showed no significant effect of sex and LPS treatment on densities of stubby and mushroom spines ( $F_{(1,20)} = 1.857$ ,  $P > 0.05$ ;  $F_{(1,20)} = 0.163$ ,  $P > 0.05$ ;  $F_{(1,20)} = 3.570$ ,  $P > 0.05$ ;  $F_{(1,20)} = 0.832$ ,  $P > 0.05$ ), but a significant effect of sex with sex  $\times$  LPS treatment interaction on the density of long-thin spines ( $F_{(1,20)} = 4.397$ ,  $P \leq 0.05$ ;  $F_{(1,20)} = 8.621$ ,  $P \leq 0.05$ , Figure 7e–g) with the partial  $\eta^2$  of 0.18. The density of long-thin spines was increased in males after LPS injection ( $P \leq 0.05$ , Figure 7f). There was a negative correlation between time spent in stimulus chamber and density of thin and mushroom spines ( $r = -0.580$ ,  $P \leq 0.05$ ;  $r = -0.520$ ,  $P \leq 0.05$ ) (Figure S5B,C).

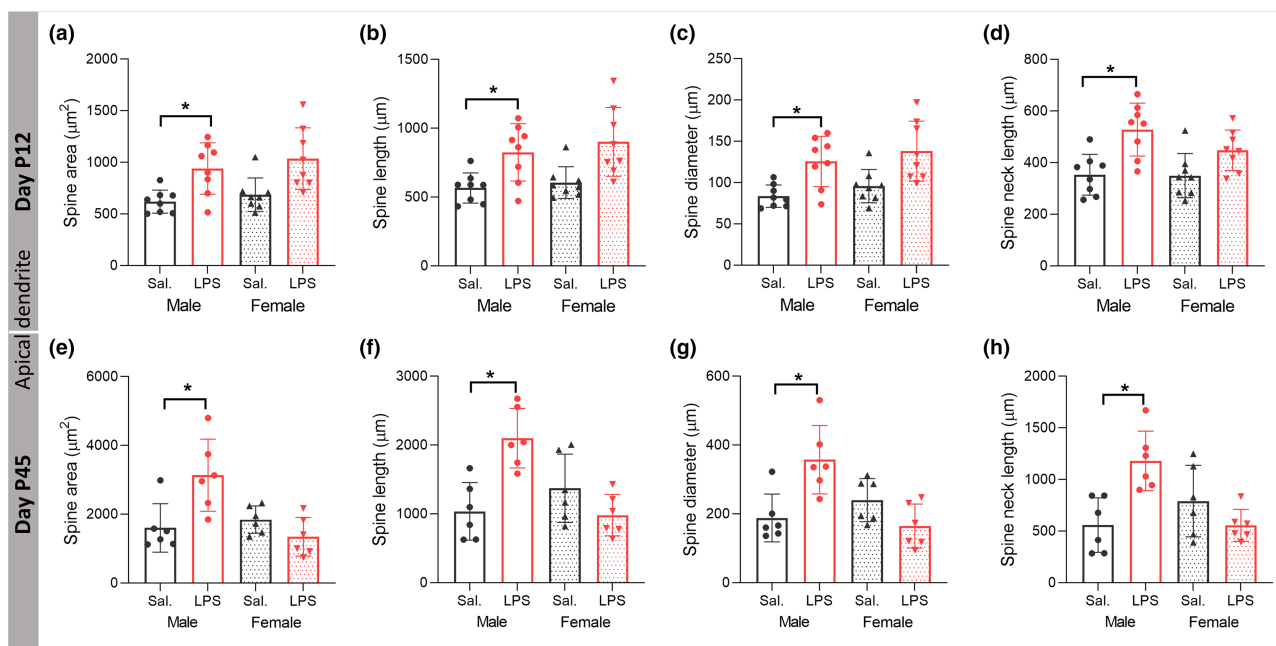


**FIGURE 6** Postnatal immune activation (PIA) remodels spine morphology of pyramidal neurons in the CA1 area of hippocampus in a time- and sex-dependent manner. Morphology of spines, including spine area (a, e), spine length (b, f), spine diameter (c, g), and spine neck length (d, h), was investigated on 3-D reconstructed apical dendrites on Golgi-Cox impregnated pyramidal neurons in the CA1 subregion of hippocampus in mice at P12 (a–d) ( $N = 8$  per group) and P45 ( $N = 6$  per group) (e–h). Spine area, length, diameter, and neck length were enlarged in PIA males at P12 and P45. Two-way ANOVA with Games-Howell and Tukey post hoc tests were used for the statistical analysis. \* $P \leq 0.05$

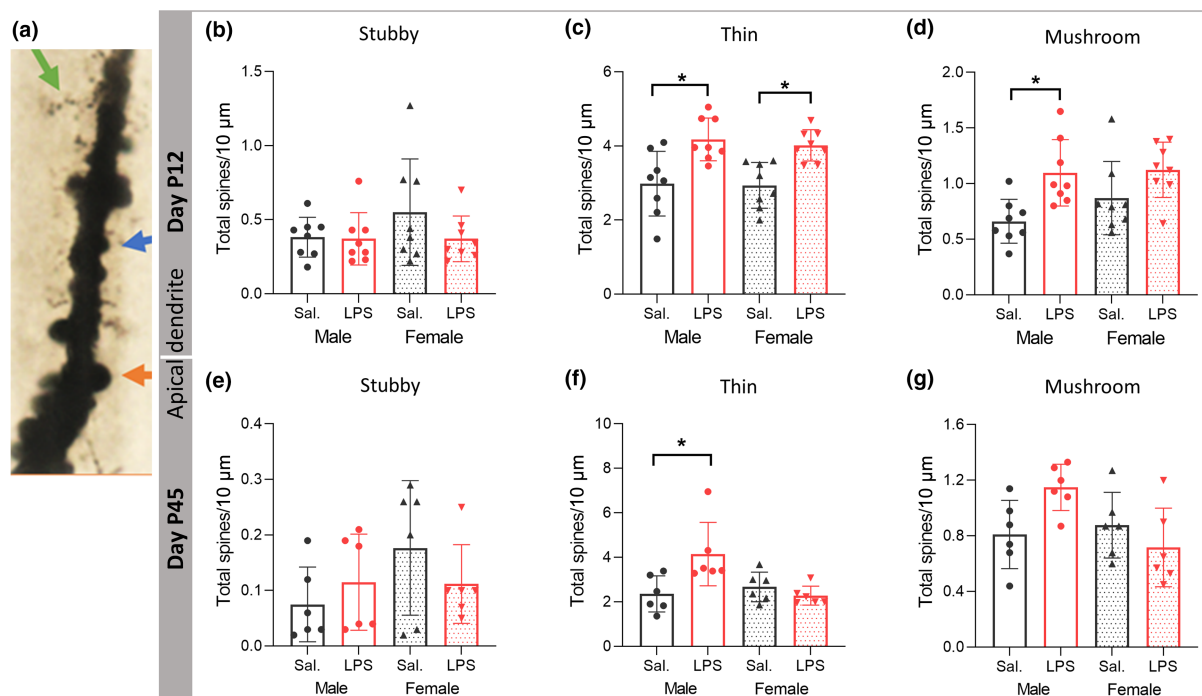


**FIGURE 7** Postnatal immune activation (PIA) alters density of different types of spines of pyramidal neurons in the CA1 area of hippocampus in a time- and sex-dependent manner. Density of spine types, including long-thin (green arrow), mushroom (orange arrow) and stubby (blue arrow) (a), was investigated on 3-D reconstructed apical dendrites on Golgi-Cox impregnated pyramidal neurons in the CA1 subregion of hippocampus in mice at P12 (b–d) ( $N = 8$ /group) and P45 ( $N = 6$  per group) (e–g). The density of stubby spines was not different between groups at P12 (b) or P45 (e). Density of long-thin spines was increased in both PIA male and female mice at P12 (c), but only in PIA males at P45 (f). The density of mushroom spines was increased in PIA males only at P12 (d). Two-way ANOVA with Tukey post hoc test was used for the statistical analysis. \* $P \leq 0.05$

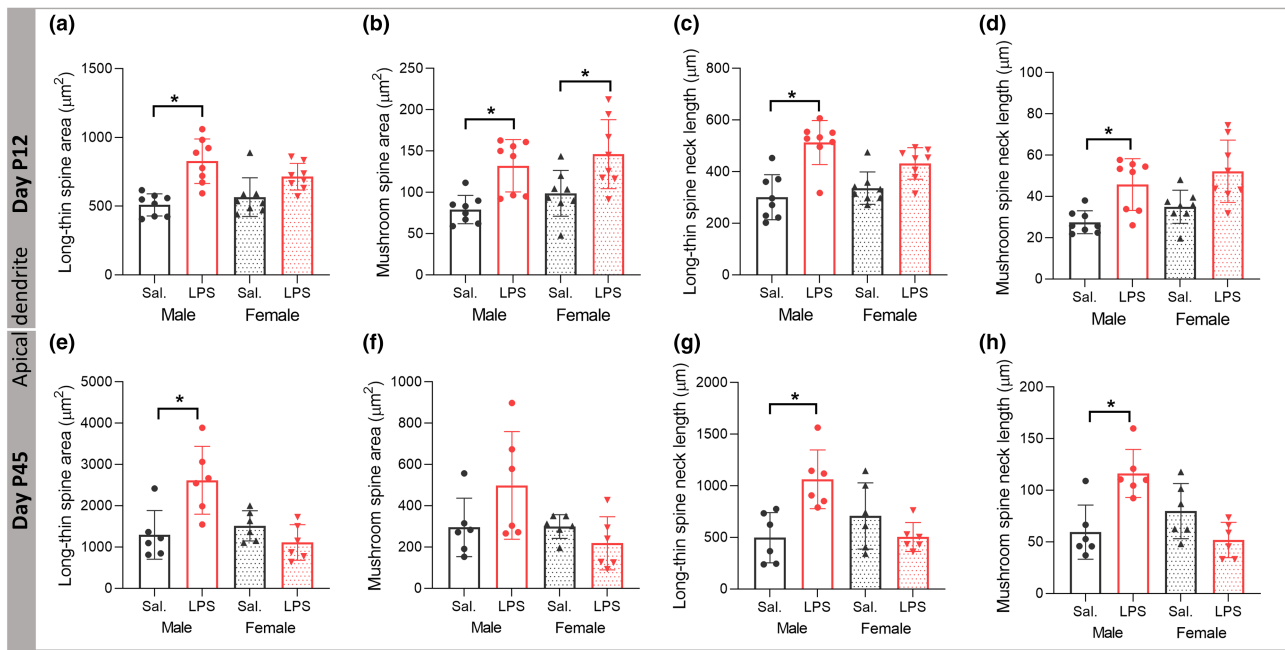


**FIGURE 8** Postnatal immune activation (PIA) remodels morphology of different types of spines of pyramidal neurons in the CA1 area of hippocampus in a time- and sex-dependent manner. Morphology of long-thin (a, c, e, g) and mushroom (b, d, f, h) spines, including spine area (a, b, e, f) and spine neck length (c, d, g, h) was investigated on 3-D reconstructed apical dendrites on Golgi-Cox impregnated pyramidal neurons in the CA1 subregion of hippocampus in mice at P12 ( $N = 8/\text{group}$ ) (a–d) and P45 ( $N = 6$  per group) (e–h). The spine area and neck length of long-thin spines was increased at P12 (a, c) and P45 (e, g) in male PIA mice. Spine area on mushroom spines was increased in both males and females at P12 (b), while neck length of mushroom spines was only increased in PIA males at P12 (d) and P45 (h). Two-way ANOVA with Tukey post hoc test was used for the statistical analysis. \* $P \leq .05$

### 3.9 | PIA remodels morphology of different types of neuronal spines in a sex-dependent manner

At P12, there was no effect of LPS treatment and sex on the area ( $F_{(1,28)} = 2.71, P > 0.05$ ;  $F_{(1,28)} = 2.688, P > 0.05$ ) or the neck length of stubby spines on apical dendrites ( $F_{(1,28)} = 2.233, P > 0.05$ ;  $F_{(1,28)} = 0.895, P > 0.05$ , data not shown). For long-thin and mushroom spines, a significant effect of LPS treatment on spine area was observed ( $F_{(1,28)} = 20.099, P \leq 0.05$ ;  $F_{(1,28)} = 21.191, P \leq 0.05$ ) with partial  $\eta^2$  of 0.50 and 0.43. The long-thin spine area was significantly larger in male LPS versus male saline ( $P \leq 0.05$ , Figure 8a) without a difference in female mice ( $P > 0.05$ , Figure 8a). Mushroom spine area was significantly larger in both male and female mice after LPS ( $P \leq 0.05$ ) (Figure 8b). Further, there was a significant effect of LPS treatment and LPS  $\times$  sex interaction on spine neck length of long-thin spines ( $F_{(1,28)} = 33.537, P \leq 0.05$ ;  $F_{(1,28)} = 4.801, P \leq 0.05$ ) with the partial  $\eta^2$  of 0.54 and of mushroom spines ( $F_{(1,28)} = 21.01, P \leq 0.05$ ) with the partial  $\eta^2$  of 0.42. Tukey post hoc analysis showed significant difference in the long-thin spine neck length in male LPS versus male saline ( $P \leq 0.05$ , Figure 8c). The Games-Howell post hoc test showed significantly larger mushroom neck length in male LPS compared with the male saline group ( $P \leq 0.05$ , Figure 8d), without changes in female mice after LPS injection ( $P > 0.05$ ).

On apical dendrites at P45, there was no effect of LPS treatment and sex on the spine area and neck length of stubby spines ( $P > 0.05$ , data not shown). The spine area was not affected on mushroom spines by LPS or sex ( $F_{(1,20)} = 0.829, P > 0.05$ ;  $F_{(1,20)} = 4.232, P > 0.05$ , Figure 8f), while there was a significant effect of sex on spine area of long-thin spines ( $F_{(1,20)} = 7.374, P \leq 0.05$ ) with the partial  $\eta^2$  of 0.26, as well as sex  $\times$  LPS treatment interaction ( $F_{(1,20)} = 13.339, P \leq 0.05$ ). Spine area on long-thin spines was significantly larger in male LPS versus male saline mice ( $P \leq 0.05$ , Figure 8e) without difference in female mice after LPS injection ( $P > 0.05$ ). There was a significant LPS  $\times$  sex interaction on spine neck length of long-thin spines ( $F_{(1,20)} = 13.571, P \leq 0.05$ ). On mushroom spines, there was a significant effect of sex on spine neck length ( $F_{(1,20)} = 5.275, P \leq 0.05$ ) with the partial  $\eta^2$  of 0.20 and sex  $\times$  LPS treatment interaction ( $F_{(1,20)} = 19.328, P \leq 0.05$ ). Tukey post hoc analysis showed significant difference in the long-thin spine neck length in male LPS versus male saline ( $P \leq 0.05$ , Figure 8g). Also, mushroom spines had a significantly larger spine neck length in male LPS compared with male saline mice ( $P \leq 0.05$ , Figure 8h), without changes in the female mice after LPS injection ( $P > 0.05$ ).

On basal dendrites, there was a significant increase in the length and area of thin spine in female mice 7 days after LPS injection without changes in the morphology of other types of spines (Figure S8).

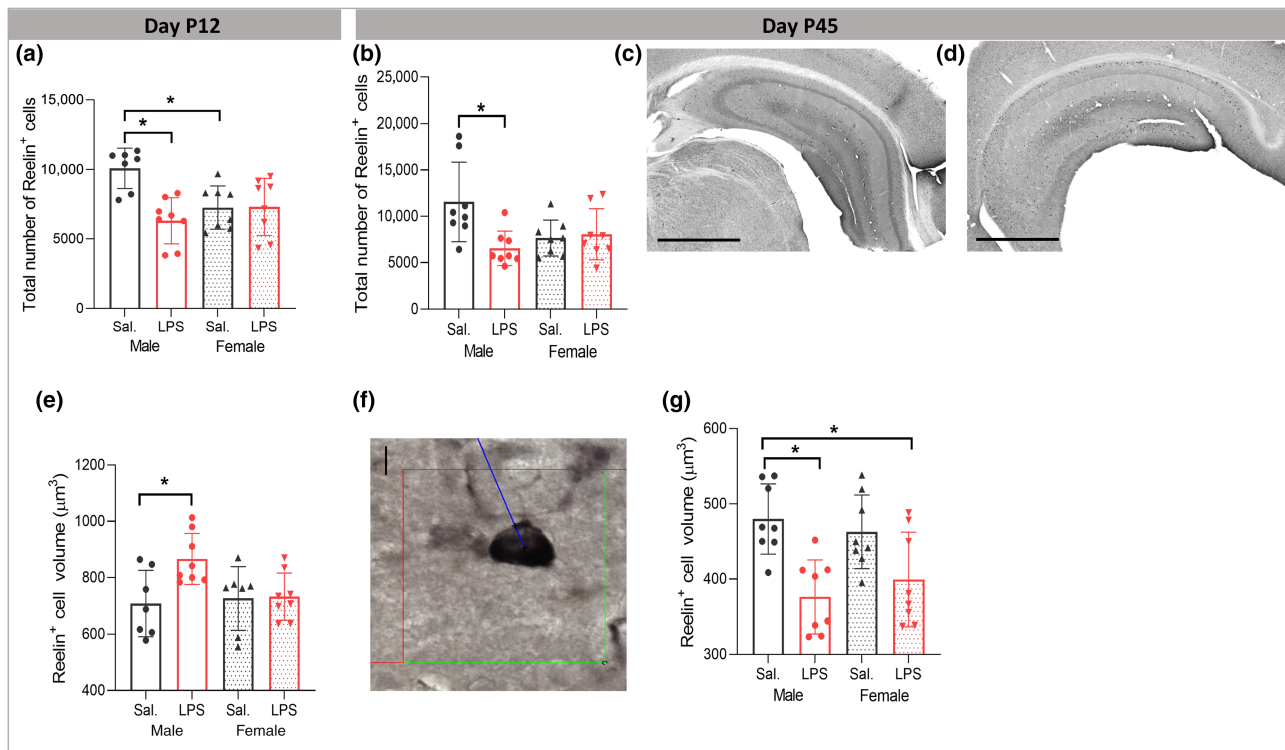


**FIGURE 9** Effects of postnatal immune activation (PIA) on Reelin<sup>+</sup> cells at P12 and P45. At P12 and P45, number (a, b) and cell soma volume (e, g) of Reelin<sup>+</sup> cells were analysed by unbiased stereological methods (f). PIA males had fewer Reelin<sup>+</sup> cells compared with saline treated males at P12 (a) and P45 (b). Examples of hippocampal sections stained with Reelin antibody in male saline (c) and male LPS (d) groups at P45. Scale bar = 1000  $\mu\text{m}$ . Reelin<sup>+</sup> cells volume was transiently increased at P12 in PIA males (e), while decreased at P45 (g). Volume measurements were determined by applying spatial rotator estimator independent of the orientation under a 100 $\times$  objective lens (f). Scale bar = 35  $\mu\text{m}$  (d). ( $N = 8$  per group). Two-way ANOVA with Tukey post hoc test was used for the statistical analysis. \* $P \leq 0.05$

### 3.10 | PIA alters morphology and number of Reelin<sup>+</sup> cells in the CA1 area of the hippocampus in a sex-dependent manner

Reelin plays a vital role in synaptic plasticity during development and has been studied as a potential biomarker for autism (Folsom & Fatemi, 2013), and as such, we examined morphological and numerical alteration of Reelin<sup>+</sup> cells following PIA (Figure 9c,d,f). At P12, our results showed a significant LPS  $\times$  sex interaction ( $F_{(1,27)} = 5.305$ ,  $P \leq 0.05$ ) with the significant main effect of LPS ( $F_{(1,27)} = 6.501$ ,  $P \leq 0.05$ ) on the number of Reelin<sup>+</sup> cells with the partial  $\eta^2$  of 0.19. Tukey post hoc analysis demonstrated a selective decrease in the number of Reelin<sup>+</sup> cells in male LPS group compared with male saline mice ( $P \leq 0.05$ , Figure 9a), without significant numerical change in female mice ( $P > 0.05$ ). At the baseline level, there was a significantly higher number of Reelin<sup>+</sup> cells in male saline group versus female saline group ( $P \leq 0.05$ , Figure 9a).

Two-way ANOVA analysis showed significant LPS  $\times$  sex interaction ( $F_{(1,29)} = 4.215$ ,  $P \leq 0.05$ ) on the volume of Reelin<sup>+</sup> cells with the main effect of treatment ( $F_{(1,29)} = 4.932$ ,  $P \leq 0.05$ ). Partial  $\eta^2$  for the effect of treatment was 0.15 which indicated a large effect of LPS treatment on the volume of Reelin<sup>+</sup> cells. Tukey post hoc analysis revealed

that at the baseline, there was no difference in the volume of the Reelin<sup>+</sup> cells in the CA1 area between male and female saline mice ( $P > 0.05$ ); however, the volume of Reelin<sup>+</sup> cells in male LPS was significantly larger than male saline mice ( $P \leq 0.05$ ), while no difference was observed in female mice after perinatal LPS injection (Figure 9e).

At P45, we found a significant LPS  $\times$  sex interaction ( $F_{(1,27)} = 7.042$ ,  $P \leq 0.05$ ) with the significant main effect of LPS ( $F_{(1,27)} = 5.104$ ,  $P \leq 0.05$ ) on the number of Reelin<sup>+</sup> cells with the partial  $\eta^2$  of 0.20. Tukey post hoc analysis identified a selective decrease in male LPS group compared with the male saline mice ( $P \leq 0.05$ ) without significant numerical change in the female mice ( $P > 0.05$ ) (Figure 9b). Two-way ANOVA analysis showed significant main effect of LPS on the volume of Reelin<sup>+</sup> cells at P45 ( $F_{(1,31)} = 20.360$ ,  $P \leq 0.05$ ) with the partial  $\eta^2$  of 0.42 which indicated a large effect of LPS treatment on the volume of Reelin<sup>+</sup> cells. The volume of Reelin<sup>+</sup> cells in male LPS group was significantly smaller than in the male saline group ( $P \leq 0.05$ , Figure 9g), with no significant change in LPS injected females compared with female saline group ( $P > 0.05$ , Figure 9g). We found a significant positive correlation between time spent in stimulus mouse chamber and the volume of Reelin<sup>+</sup> cells ( $r = 0.607$ ,  $P \leq 0.05$ ), without significant correlation with changes in the number of Reelin<sup>+</sup> cells ( $r = 0.325$ ,  $P > 0.05$ ).

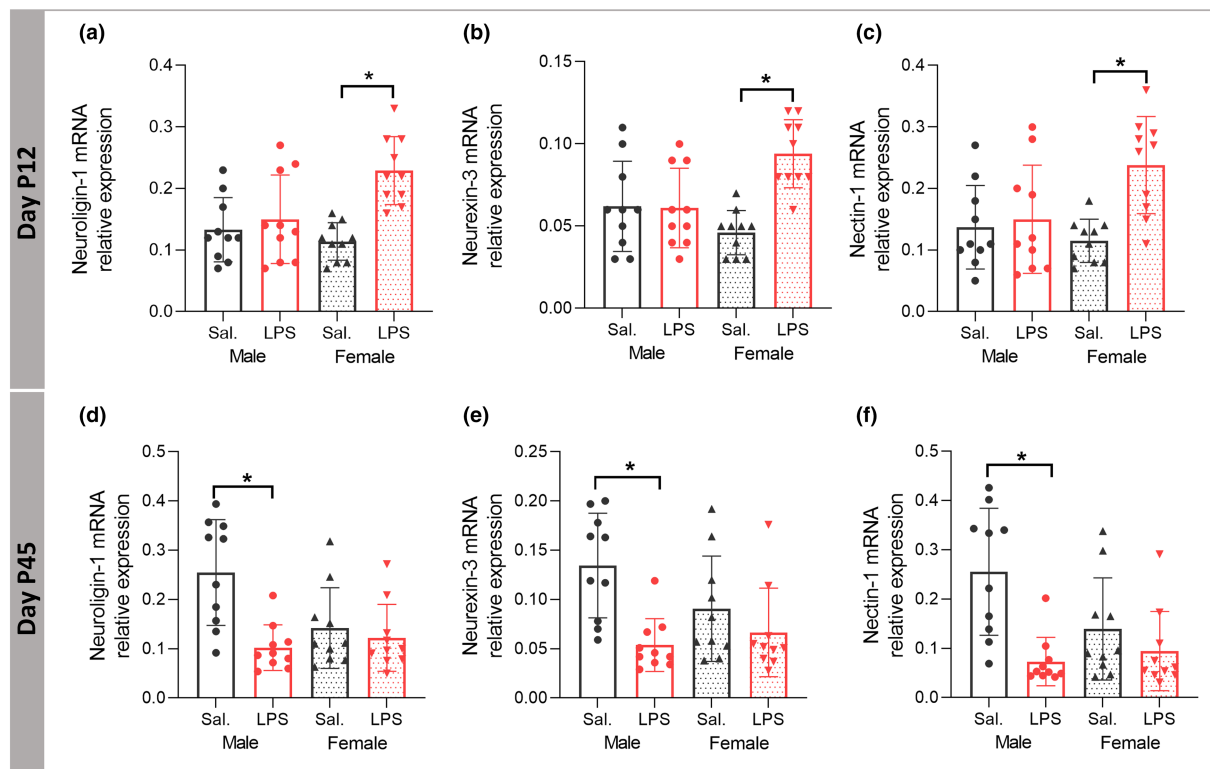


**FIGURE 10** Effects of postnatal immune activation (PIA) on synaptic cell adhesion mRNA expression at P12 and P45. Levels of mRNA expression for neuroigin-1 (NLGN1), neurexin-3 (NRXN-3), and Nectin-1 were determined by RT-PCR in the hippocampus at P12 (a–c) and P45 (d–f). NLGN1, NRXN-3, and Nectin-1 mRNA expression were significantly increased in female PIA at P12 (a–c), while the mRNA expression for all three genes was decreased in male PIA at P45 (d–f). ( $N = 10$  per group). Two-way ANOVA with Games-Howell and Tukey post hoc tests were used for the statistical analysis. \* $P \leq 0.05$

### 3.11 | PIA reduces hippocampal mRNA expression of trans-synaptic and cellular adhesion molecules in a sex-dependent manner

Reelin-signalling regulates presynaptic and postsynaptic structure/function by impinging trans-synaptic adhesion proteins. Therefore, we studied presynaptic NRXN3, postsynaptic NLGN1 and nectin-1. At P12, two-way ANOVA analysis demonstrated a significant LPS  $\times$  sex interaction on hippocampal mRNA expression of NLGN1 ( $F_{(1,36)} = 8.214$ ,  $P \leq 0.05$ ) with a significant main effect of LPS treatment ( $F_{(1,36)} = 14.096$ ,  $P \leq 0.05$ ) and the partial  $\eta^2$  of 0.28. Tukey post hoc analysis showed that the mRNA expression of NLGN1 was significantly higher in female LPS compared with female saline mice ( $P \leq 0.05$ , Figure 10a), with no significant difference in male mice ( $P > 0.05$ ). Two-way ANOVA of expression of mRNA level of NRXN3 demonstrated significant LPS  $\times$  sex interaction ( $F_{(1,36)} = 12.123$ ,  $P \leq 0.05$ ), with the significant main effect of LPS treatment ( $F_{(1,36)} = 11.649$ ,  $P \leq 0.05$ ) and with the partial  $\eta^2$  of 0.24. Tukey post hoc analysis showed that mRNA level of NRXN3 was significantly higher in female LPS compared with female saline mice ( $P \leq 0.05$ , Figure 10b), with no significant difference in male mice ( $P > 0.05$ ). Two-way ANOVA of hippocampal mRNA level of nectin-1 showed significant LPS  $\times$  sex interaction ( $F_{(1,36)} = 6.574$ ,  $P \leq 0.05$ ) with the

significant main effect of LPS treatment ( $F_{(1,36)} = 9.946$ ,  $P \leq 0.05$ ) and with the partial  $\eta^2$  of 0.21. Games-Howell post hoc analysis demonstrated that the mRNA expression of nectin-1 was significantly higher in female LPS compared with female saline mice ( $P \leq 0.05$ , Figure 10c), with no significant difference in male mice ( $P > 0.05$ ).

At P45, there was a significant LPS  $\times$  sex interaction ( $F_{(1,36)} = 7.027$ ,  $P \leq 0.05$ ) with the significant main effect of LPS treatment ( $F_{(1,36)} = 11.850$ ,  $P \leq 0.05$ ) and with the partial  $\eta^2$  of 0.24 on the mRNA expression of NLGN1. Games-Howell post hoc analysis showed that the mRNA expression of NLGN1 was significantly lower in male LPS compared with the male saline mice ( $P \leq 0.05$ , Figure 10d), with no significant difference in female mice ( $P > 0.05$ ). Analysis of NRXN3 mRNA expression showed significant main effect of LPS treatment ( $F_{(1,36)} = 13.094$ ,  $P \leq 0.05$ ) with the partial  $\eta^2$  of 0.26. Tukey post hoc analysis demonstrated that NRXN3 mRNA expression was decreased in LPS males ( $P \leq 0.05$ , Figure 10e), but not in females ( $P > 0.05$ ). Two-way ANOVA analysis of nectin-1 mRNA expression showed a significant LPS  $\times$  sex interaction ( $F_{(1,36)} = 5.171$ ,  $P \leq 0.05$ ) with the significant main effect of LPS treatment ( $F_{(1,36)} = 14.198$ ,  $P \leq 0.05$ ) and the partial  $\eta^2$  of 0.28. Games-Howell post hoc analysis showed decreased mRNA expression of nectin-1 in LPS male mice ( $P \leq 0.05$ , Figure 10f) with no significant treatment effect in females ( $P > 0.05$ ).

## 4 | DISCUSSION

We show that PIA at a critical brain developmental stage in mice equivalent to preterm human infants reduces sociability and increases repetitive behaviours in P45 adolescent male animals. As shown by diffusion kurtosis MRI, a reflective marker of tissue heterogeneity, behavioural changes were associated with sex-dependent brain overgrowth and abnormal microstructure in the hippocampus together with morphological changes of hippocampal microglia consistent with activation, immaturity of neuronal spine development, and reduced number and size of Reelin<sup>+</sup> cells. Expression of trans-synaptic and cell adhesion genes was reduced in males in the long-term after PIA. Thus, the results highlight distinct sex-dependent effects of PIA on Reelin<sup>+</sup> cells, excitatory synapses and alterations in brain growth relevant for ASD.

Inflammation through TLR activation significantly contributes to ASD. In support, here we show that a single injection of LPS induced neuropathology associated with ASD-like phenotypic behaviour, suggesting that triggering immune responses early in life plays an important role in the aetiology of ASD. Similarly, a recent clinical study showed that inflammation in preterm children without severe neonatal brain lesions was associated with inferior social ability (Cogley et al., 2020; Giraud et al., 2020). Preterm infants have an increased susceptibility to infections, which may be related to their immature immune system (Currie et al., 2011; Howson et al., 2013; Wynn et al., 2009).

We found larger brain volume in LPS injected males. Clinical findings have identified brain overgrowth as an early predictor for ASD diagnosis (Hazlett et al., 2017; Shen et al., 2013). Further, persistent enlargement of hippocampus has been reported (Schumann et al., 2004), and structural abnormalities in the CA1 area of the hippocampus were highlighted in children with ASD (Li et al., 2019). In line with these findings, we show that the volume of the hippocampus is enlarged in males after LPS, and we locate the changes specifically to the CA1 SR region which may be due to increased neuropil, number of cells, arborization, or misplaced cells (heterotopia) (Raymond et al., 1996; Weidenheim et al., 2001). Diffusion tensor imaging showed that mean diffusivity probability distributions of both grey and white matter shift towards a higher value in adolescent autistic individuals (Groen et al., 2011). Similarly, we demonstrated by quantitative DKI analysis a significant change to higher values of mean diffusivity distributions in the hippocampus of adolescent male mice following neonatal LPS without significant changes in mean kurtosis. Alterations in mean diffusivity without changes in mean kurtosis have previously been interpreted to indicate increased extracellular space due to dendritic spanning volumes, rather than loss of neuronal cell bodies, synapses, or dendrites. Thus, diffusion tensor image changes observed in male LPS animals in the current study may be related to the total volume occupied by neurons as we found larger convex hulls of apical dendrites in male LPS group.

During brain development, transition from immature synapses on long thin spines to larger synapses on mushroom-shaped spines occur. We found densities of both immature thin and mature mushroom spines increased on apical dendrites in paediatric male LPS mice, but only the increase in thin spines remained until adolescent age.

Similarly, age-dependent transient increase in perforated hippocampal synapses, mainly comprised of mushroom spines, has been observed in Shank3 mutant mice (Uppal et al., 2015). Synapse maturation is dependent on spine pruning by microglia (Mallya et al., 2019). However, our results suggest that increased thin spine density, specifically in male LPS injected mice, was unlikely to be due to microglia pruning, at least alone, since we observed activated microglia in both male and female LPS mice. A previous study reported greater spine density in the cortex in ASD due to lesser synapse pruning by impaired autophagy (Tang et al., 2014; Werling et al., 2016) suggesting that other mechanisms than microglia pruning may be involved.

Spine geometry reflects spine function and correlates with release probability of vesicles in the synapses (Nimchinsky et al., 2002) and long-term potentiation (LTP) (Gipson & Olive, 2017). LTP induction promotes spine head enlargement, and stabilization of new spines (Chidambaram et al., 2019). Thus, our finding of an increased density and size of thin spines in adolescent PIA male mice suggest lack of synapse maturation with enhanced LTP. The correlation between spine neck length and synaptic efficacy is inverse, therefore longer spine neck results in negligible somatic voltage contributions, while shortening of spine neck leads to increases in synaptic efficacy (Araya et al., 2014). The current data support this finding, as only male LPS mice exhibited longer spine necks on apical dendrites without differences in female mice.

To determine the possible underlying cellular mechanisms of the changes in synapse development, we investigated Reelin<sup>+</sup> cells, which are essential for forming layer-specific hippocampal connections during development and have been implicated in ASD (Lammert & Howell, 2016). We found that male LPS mice had fewer Reelin<sup>+</sup> cells in the hippocampus at P12 and P45 and smaller soma at P45 than saline-injected animals. These findings are in line with a study that showed lower reelin expression in the brain from subjects with ASD (Fatemi, 2001, 2002). The reason for the reduced number of Reelin<sup>+</sup> cells in males is unclear but could be due to sex-dependent microglia phagocytosis of neuronal cells as there is evidence from a model of androgen-induced microglia phagocytosis that microglia engulf proliferating cells in a sex-dependent manner (VanRyzin et al., 2019). In support, we have previously shown that neonatal LPS inhibits neurogenesis and neuronal maturation (Smith et al., 2014), although whether this is sex-dependent remains to be investigated. Reelin also modulates GABA-B receptor signalling (Hamad et al., 2021), which is expressed by microglia (Kuhn et al., 2004) and links microglia to neuronal activity in the hippocampus during the postnatal period (Loggiacco et al., 2021). Thus, it is possible that fewer and smaller Reelin<sup>+</sup> cells in the current study have affected the communication between microglia and neurons, which could be important for the behavioural changes we observed.

There were age dependent effects on Reelin<sup>+</sup> cell soma volume, with increased volume at P12 in male LPS mice. Hypothetically, at P12 (the developmental period) the increase in the size may reflect increased activity in response to the novel environmental stimulus (LPS) as during early postnatal development, Reelin activity contributes to the PI3K-Akt-mTOR pathway underlying dendrite outgrowth and spine development (Lee & D'Arcangelo, 2016). Therefore, bigger

size of Reelin<sup>+</sup> cells may be representative of higher activity, but further studies are needed to explore this in more detail.

Reelin mediates interactions between two of the most prominent trans-synaptic genes (NLGN and NRXN) (Niu et al., 2004). Therefore, we examined the gene expression of NLGN1, NRXN-3, and nectin-1, which have been implicated in the differentiation and maturation of both excitatory and inhibitory synapses (Bottos et al., 2009; Krueger et al., 2012) and important for ASD (Sudhof, 2008). While there was a transient early increase in females, LPS-treated males demonstrated a long-term decrease in expression of all three genes. These findings agree with previous studies that found decreased expression of NRXN3 mRNA in male fragile X knockout (FMR1-KO) mice while expression was increased in females (Lai et al., 2016). NLGNs have a critical role in the balance of inhibitory and excitatory transmission, and mice with NLGN1 deletion exhibited repetitive stereotyped grooming behaviours (Blundell et al., 2010). Nectin-1 is expressed on CR cells during development (Gil-Sanz et al., 2013; Lim et al., 2008; Rikitake et al., 2012), and reelin has been shown to promote the assembly of Nectin-1 adhesion sites (Gil-Sanz et al., 2013). Collectively, our results highlight trans-synaptic adhesion proteins as one of the molecular targets of sex-dependent effects by PIA that may underlie the defect in spine maturation observed.

Our results demonstrate that immune activation by LPS early in neonatal life has a sex-dependent effect on ASD-like behaviour in mice. In support, studies have shown that prenatal LPS exposure during the last two-thirds of gestation result in impairment in social interactions and exploration in male mice (Basta-Kaim et al., 2015; Carlezon et al., 2019; Taylor et al., 2012). Alteration of immune pathways, including IL-17 and NFK-B, in the hippocampus following perinatal immune activation has been suggested to underlie autistic-like behaviours (Choi et al., 2016). Similarly, expression of pro-inflammatory cytokines was found in the brains and serum of patients with autism (Chez et al., 2007; Ratnayake et al., 2013). In the current study, while we did not examine specific inflammatory pathways, we did find increased number of the resident immune cells in the brain and microglia in male mice 40 days after LPS injection, suggesting a stronger immune response. This is in line with our previous study showing increased microglia proliferation after neonatal LPS exposure (Smith et al., 2014). Taken together, studies demonstrate that inflammation both before and after birth is an important etiological factor for inferior social ability by considering dysregulation of immune-related genes and changes in the activation of neuroimmune cells.

The current study provides novel sex-dependent insights into synapse remodelling in the hippocampus in an animal model of post-natal inflammation with autism phenotype. We propose that the sex-dependent deficiency in Reelin<sup>+</sup> cells and abnormal regulation of NLGN-1, NRXN3, and nectin-1 contribute to an impaired maturation of neuronal spines resulting in an excitatory/inhibitory imbalance at the synapse, thereby increasing the risk for autistic-like behaviour in males. These findings give important new cellular and molecular information on possible underlying mechanisms of the interaction of infection in preterm male infants and brain development that may underlie autistic-like behaviour.

## ACKNOWLEDGEMENTS

This study was supported by Lundbeck Foundation (R322-2019-2721), Mary von Sydows Foundation (2020-3420), Magn. Bergvalls Foundation (2020-03756), HKH Kronprinsessan Lovisas Foundation, Axel Tielmans Foundation (2020-00559), Frimurare Barnhusdirektionen, Wilhelm och Martina Lundgrens Vetenskapsfond, Swedish Research Council (VR-2017-01409), Åhlen Foundation, Public Health Service at the Sahlgrenska University Hospital (ALFGBG-722491), Swedish Brain Foundation (FO2019-0270), and National Institute of Health (R01 HL139685; R01 NS103483).

## AUTHOR CONTRIBUTIONS

CM, MA, GW, and LW designed the study. MA, TC, AQ, EH, ALR, GG, AMJS, PS, SA, and BH performed the experiments, data collection, and data analysis. CM, MA, GW, and LW interpreted the results and wrote the manuscript. All authors provided the conceptual advice, commented on the manuscript, and approved the final version of the manuscript for submission.

## CONFLICT OF INTEREST

The authors have nothing to disclose.

## DECLARATION OF TRANSPARENCY AND SCIENTIFIC RIGOUR

This Declaration acknowledges that this paper adheres to the principles for transparent reporting and scientific rigour of preclinical research as stated in the *BJP* guidelines for [Design and Analysis](#), [Immunoblotting and Immunochemistry](#), and [Animal Experimentation](#), and as recommended by funding agencies, publishers and other organizations engaged with supporting research.

## DATA AVAILABILITY STATEMENT

The data that support the findings of this study are available from the corresponding author upon request.

## REFERENCES

- Alexander, C., & Rietschel, E. T. (2001). Bacterial lipopolysaccharides and innate immunity. *Journal of Endotoxin Research*, 7(3), 167–202. <https://doi.org/10.1179/096805101101532675>
- Alexander, S. P., Christopoulos, A., Davenport, A. P., Kelly, E., Mathie, A., Peters, J. A., Veale, E. L., Armstrong, J. F., Faccenda, E., Harding, S. D., Pawson, A. J., Southan, C., Davies, J. A., Abbracchio, M. P., CGTP Collaborators, Alexander, W., Al-hosaini, K., Bäck, M., Barnes, N. M., ... Ye, R. D. (2021). THE CONCISE GUIDE TO PHARMACOLOGY 2021/22: G protein-coupled receptors. *British Journal of Pharmacology*, 178(S1), S27–S156. <https://doi.org/10.1111/bph.15538>
- Alexander, S. P., Fabbro, D., Kelly, E., Mathie, A., Peters, J. A., Veale, E. L., Armstrong, J. F., Faccenda, E., Harding, S. D., Pawson, A. J., Southan, C., Davies, J. A., Beuve, A., Brouckaert, P., Bryant, C., Burnett, J. C., Farndale, R. W., Friebe, A., Garthwaite, J., ... Waldman, S. A. (2021). THE CONCISE GUIDE TO PHARMACOLOGY 2021/22: Catalytic receptors. *British Journal of Pharmacology*, 178(S1), S264–S312. <https://doi.org/10.1111/bph.15541>
- Alexander, S. P. H., Roberts, R. E., Broughton, B. R. S., Sobey, C. G., George, C. H., Stanford, S. C., Cirino, G., Docherty, J. R.,

- Giembycz, M. A., Hoyer, D., Insel, P. A., Izzo, A. A., Ji, Y., MacEwan, D. J., Mangum, J., Wonnacott, S., & Ahluwalia, A. (2018). Goals and practicalities of immunoblotting and immunohistochemistry: A guide for submission to the British Journal of Pharmacology. *British Journal of Pharmacology*, 175(3), 407–411. <https://doi.org/10.1111/bph.14112>
- Araya, R., Vogels, T. P., & Yuste, R. (2014). Activity-dependent dendritic spine neck changes are correlated with synaptic strength. *Proceedings of the National Academy of Sciences of the United States of America*, 111(28), E2895–E2904. <https://doi.org/10.1073/pnas.1321869111>
- Ardalan, M., Chumak, T., Vexler, Z., & Mallard, C. (2019). Sex-dependent effects of perinatal inflammation on the brain: Implication for neuropsychiatric disorders. *International Journal of Molecular Sciences*, 20(9), 2270. <https://doi.org/10.3390/ijms20092270>
- Ardalan, M., Rafati, A. H., Nyengaard, J. R., & Wegener, G. (2017). Rapid antidepressant effect of ketamine correlates with astroglial plasticity in the hippocampus. *British Journal of Pharmacology*, 174(6), 483–492. <https://doi.org/10.1111/bph.13714>
- Ardalan, M., Wegener, G., Polsinelli, B., Madsen, T. M., & Nyengaard, J. R. (2016). Neurovascular plasticity of the hippocampus one week after a single dose of ketamine in genetic rat model of depression. *Hippocampus*, 26(11), 1414–1423. <https://doi.org/10.1002/hipo.22617>
- Basta-Kaim, A., Fijał, K., Ślusarczyk, J., Trojan, E., Głombik, K., Budziszewska, B., Leśkiewicz, M., Regulska, M., Kubera, M., Lasoń, W., & Wędzony, K. (2015). Prenatal administration of lipopolysaccharide induces sex-dependent changes in glutamic acid decarboxylase and parvalbumin in the adult rat brain. *Neuroscience*, 287, 78–92. <https://doi.org/10.1016/j.neuroscience.2014.12.013>
- Blencowe, H., Cousens, S., Chou, D., Oestergaard, M., Say, L., Moller, A. B., Kinney, M., Lawn, J., & the Born Too Soon Preterm Birth Action Group (see acknowledgement for full list). (2013). Born too soon: The global epidemiology of 15 million preterm births. *Reproductive Health*, 10(Suppl 1), S2. <https://doi.org/10.1186/1742-4755-10-S1-S2>
- Blundell, J., Blaiss, C. A., Etherton, M. R., Espinosa, F., Tabuchi, K., Walz, C., Bolliger, M. F., Sudhof, T. C., & Powell, C. M. (2010). Neuroligin-1 deletion results in impaired spatial memory and increased repetitive behavior. *The Journal of Neuroscience*, 30(6), 2115–2129. <https://doi.org/10.1523/JNEUROSCI.4517-09.2010>
- Boche, D., Perry, V. H., & Nicoll, J. A. (2013). Review: Activation patterns of microglia and their identification in the human brain. *Neuropathology and Applied Neurobiology*, 39(1), 3–18. <https://doi.org/10.1111/nan.12011>
- Bottos, A., Destro, E., Rissone, A., Graziano, S., Cordara, G., Assenzio, B., Cera, M. R., Mascia, L., Bussolino, F., & Arese, M. (2009). The synaptic proteins neurexins and neuroligins are widely expressed in the vascular system and contribute to its functions. *Proceedings of the National Academy of Sciences of the United States of America*, 106(49), 20782–20787. <https://doi.org/10.1073/pnas.0809510106>
- Carlezon, W. A. Jr., Kim, W., Missig, G., Finger, B. C., Landino, S. M., Alexander, A. J., Mokler, E. L., Robbins, J. O., Li, Y., Bolshakov, V. Y., McDougle, C. J., & Kim, K. S. (2019). Maternal and early postnatal immune activation produce sex-specific effects on autism-like behaviors and neuroimmune function in mice. *Scientific Reports*, 9(1), 16928. <https://doi.org/10.1038/s41598-019-53294-z>
- Chaddad, A., Desrosiers, C., Hassan, L., & Tanougast, C. (2017). Hippocampus and amygdala radiomic biomarkers for the study of autism spectrum disorder. *BMC Neuroscience*, 18(1), 52. <https://doi.org/10.1186/s12868-017-0373-0>
- Cheong, J. L. Y., Anderson, P. J., Burnett, A. C., Roberts, G., Davis, N., Hickey, L., Carse, E., Doyle, L. W., & for the Victorian Infant Collaborative Study Group. (2017). Changing neurodevelopment at 8 years in children born extremely preterm since the 1990s. *Pediatrics*, 139(6), e20164086. <https://doi.org/10.1542/peds.2016-4086>
- Chez, M. G., Dowling, T., Patel, P. B., Khanna, P., & Kominsky, M. (2007). Elevation of tumor necrosis factor-alpha in cerebrospinal fluid of autistic children. *Pediatric Neurology*, 36(6), 361–365. <https://doi.org/10.1016/j.pediatrneurol.2007.01.012>
- Chidambaram, S. B., Rathipriya, A. G., Bolla, S. R., Bhat, A., Ray, B., Mahalakshmi, A. M., Manivasagam, T., Thenmozhi, A. J., Essa, M. M., Guillemain, G. J., Chandra, R., & Sakharkar, M. K. (2019). Dendritic spines: Revisiting the physiological role. *Progress in Neuro-Psychopharmacology & Biological Psychiatry*, 92, 161–193. <https://doi.org/10.1016/j.pnpbp.2019.01.005>
- Choi, G. B., Yim, Y. S., Wong, H., Kim, S., Kim, H., Kim, S. V., Hoeffler, C. A., Littman, D. R., & Huh, J. R. (2016). The maternal interleukin-17a pathway in mice promotes autism-like phenotypes in offspring. *Science*, 351(6276), 933–939. <https://doi.org/10.1126/science.aad0314>
- Christensen, D. L., Maenner, M. J., Bilder, D., Constantino, J. N., Daniels, J., Durkin, M. S., Fitzgerald, R. T., Kurzius-Spencer, M., Pettygrove, S. D., Robinson, C., Shenouda, J., White, T., Zahorodny, W., Pazol, K., & Dietz, P. (2019). Prevalence and characteristics of autism Spectrum disorder among children aged 4 years - early autism and developmental disabilities monitoring network, seven sites, United States, 2010, 2012, and 2014. *MMWR Surveillance Summaries*, 68(2), 1–19. <https://doi.org/10.15585/mmwr.ss6802a1>
- Cogley, C., O'Reilly, H., Bramham, J., & Downes, M. (2020). A systematic review of the risk factors for autism Spectrum disorder in children born preterm. *Child Psychiatry & Human Development*, 52, 841–855. <https://doi.org/10.1007/s10578-020-01071-9>
- Currie, A. J., Curtis, S., Strunk, T., Riley, K., Liyanage, K., Prescott, S., Doherty, D., Simmer, K., Richmond, P., & Burgner, D. (2011). Preterm infants have deficient monocyte and lymphocyte cytokine responses to group B streptococcus. *Infection and Immunity*, 79(4), 1588–1596. <https://doi.org/10.1128/iai.00535-10>
- Curtis, M. J., Alexander, S., Cirino, G., Docherty, J. R., George, C. H., Giembycz, M. A., Hoyer, D., Insel, P. A., Izzo, A. A., Ji, Y., MacEwan, D. J., Sobey, C. G., Stanford, S. C., Teixeira, M. M., Wonnacott, S., & Ahluwalia, A. (2018). Experimental design and analysis and their reporting II: Updated and simplified guidance for authors and peer reviewers. *British Journal of Pharmacology*, 175(7), 987–993. <https://doi.org/10.1111/bph.14153>
- Custódio, C. S., Mello, B. S. F., Filho, A., de Carvalho Lima, C. N., Cordeiro, R. C., Miyajima, F., Réus, G. Z., Vasconcelos, S. M. M., Barichello, T., Quevedo, J., de Oliveira, A. C., de Lucena, D. F., & Macedo, D. S. (2018). Neonatal immune challenge with lipopolysaccharide triggers long-lasting sex- and age-related behavioral and immune/neurotrophic alterations in mice: Relevance to autism Spectrum disorders. *Molecular Neurobiology*, 55(5), 3775–3788. <https://doi.org/10.1007/s12035-017-0616-1>
- Deacon, R. M. (2006). Digging and marble burying in mice: Simple methods for in vivo identification of biological impacts. *Nature Protocols*, 1(1), 122–124. <https://doi.org/10.1038/nprot.2006.20>
- Enstrom, A. M., Onore, C. E., Van de Water, J. A., & Ashwood, P. (2010). Differential monocyte responses to TLR ligands in children with autism spectrum disorders. *Brain, Behavior, and Immunity*, 24(1), 64–71. <https://doi.org/10.1016/j.bbi.2009.08.001>
- Fatemi, S. H. (2001). Reelin mutations in mouse and man: From reeler mouse to schizophrenia, mood disorders, autism and lissencephaly. *Molecular Psychiatry*, 6(2), 129–133. <https://doi.org/10.1038/sj.mp.4000129>
- Fatemi, S. H. (2002). The role of Reelin in pathology of autism. *Molecular Psychiatry*, 7(9), 919–920. <https://doi.org/10.1038/sj.mp.4001248>
- Fereshetyan, K., Chavushyan, V., Danielyan, M., & Yenkyan, K. (2021). Assessment of behavioral, morphological and electrophysiological changes in prenatal and postnatal valproate induced rat models of autism spectrum disorder. *Scientific Reports*, 11(1), 23471. <https://doi.org/10.1038/s41598-021-02994-6>

- Folsom, T. D., & Fatemi, S. H. (2013). The involvement of Reelin in neurodevelopmental disorders. *Neuropharmacology*, *68*, 122–135. <https://doi.org/10.1016/j.neuropharm.2012.08.015>
- Gil-Sanz, C., Franco, S. J., Martinez-Garay, I., Espinosa, A., Harkins-Perry, S., & Muller, U. (2013). Cajal-Retzius cells instruct neuronal migration by coincidence signaling between secreted and contact-dependent guidance cues. *Neuron*, *79*(3), 461–477. <https://doi.org/10.1016/j.neuron.2013.06.040>
- Gipson, C. D., & Olive, M. F. (2017). Structural and functional plasticity of dendritic spines - root or result of behavior? *Genes, Brain, and Behavior*, *16*(1), 101–117. <https://doi.org/10.1111/gbb.12324>
- Giraud, A., Chauv, R., Allard, M.-J., Celle, M., Teyssier, G., Roche, F., Chapelle, C., Chabrier, S., Sébire, G., & Patural, H. (2020). Perinatal inflammation is associated with social and motor impairments in pre-term children without severe neonatal brain injury. *European Journal of Paediatric Neurology*, *28*, 126–132. <https://doi.org/10.1016/j.ejpn.2020.06.008>
- Glessner, J. T., Wang, K., Cai, G., Korvatska, O., Kim, C. E., Wood, S., Zhang, H., Estes, A., Brune, C. W., Bradfield, J. P., Imielinski, M., Frackelton, E. C., Reichert, J., Crawford, E. L., Munson, J., Sleiman, P. M. A., Chiavacci, R., Annaiah, K., Thomas, K., ... Hakonarson, H. (2009). Autism genome-wide copy number variation reveals ubiquitin and neuronal genes. *Nature*, *459*(7246), 569–573. <https://doi.org/10.1038/nature07953>
- Groen, W. B., Buitelaar, J. K., van der Gaag, R. J., & Zwiers, M. P. (2011). Pervasive microstructural abnormalities in autism: A DTI study. *Journal of Psychiatry & Neuroscience*, *36*(1), 32–40. <https://doi.org/10.1503/jpn.090100>
- Gundersen, H. J. (1986). Stereology of arbitrary particles. A review of unbiased number and size estimators and the presentation of some new ones, in memory of William R. Thompson. *Journal of Microscopy*, *143*(Pt 1), 3–45. <https://doi.org/10.1111/j.1365-2818.1986.tb02764.x>
- Gundersen, H. J. (2002). The smooth fractionator. *Journal of Microscopy*, *207*(Pt 3), 191–210. <https://doi.org/10.1046/j.1365-2818.2002.01054.x>
- Gundersen, H. J., Bagger, P., Bendtsen, T. F., Evans, S. M., Korbo, L., Marcussen, N., MØLLer, A., Nielsen, K., Nyengaard, J. R., Pakkenberg, B., SØrensen, F. B., Vesterby, A., & West, M. J. (1988). The new stereological tools: Disector, fractionator, nucleator and point sampled intercepts and their use in pathological research and diagnosis. *APMIS*, *96*(10), 857–881. <https://doi.org/10.1111/j.1699-0463.1988.tb00954.x>
- Hagberg, H., Gressens, P., & Mallard, C. (2012). Inflammation during fetal and neonatal life: Implications for neurologic and neuropsychiatric disease in children and adults. *Annals of Neurology*, *71*(4), 444–457. <https://doi.org/10.1002/ana.22620>
- Hagberg, H., Mallard, C., Ferriero, D. M., Vannucci, S. J., Levison, S. W., Vexler, Z. S., & Gressens, P. (2015). The role of inflammation in perinatal brain injury. *Nature Reviews. Neurology*, *11*(4), 192–208. <https://doi.org/10.1038/nrneurol.2015.13>
- Haida, O., al Sagheer, T., Balbous, A., Francheteau, M., Matas, E., Soria, F., Fernagut, P. O., & Jaber, M. (2019). Sex-dependent behavioral deficits and neuropathology in a maternal immune activation model of autism. *Translational Psychiatry*, *9*(1), 124. <https://doi.org/10.1038/s41398-019-0457-y>
- Hallmayer, J., Cleveland, S., Torres, A., Phillips, J., Cohen, B., Torigoe, T., Miller, J., Fedele, A., Collins, J., Smith, K., Lotspeich, L., Croen, L. A., Ozonoff, S., Lajonchere, C., Grether, J. K., & Risch, N. (2011). Genetic heritability and shared environmental factors among twin pairs with autism. *Archives of General Psychiatry*, *68*(11), 1095–1102. <https://doi.org/10.1001/archgenpsychiatry.2011.76>
- Hamad, M. I. K., Jbara, A., Rabaya, O., Petrova, P., Daoud, S., Melliti, N., Meseke, M., Lutz, D., Petrasch-Parwez, E., Schwitalla, J. C., Mark, M. D., Herlitze, S., Reiss, G., Herz, J., & Förster, E. (2021). Reelin signaling modulates GABAB receptor function in the neocortex. *Journal of Neurochemistry*, *156*(5), 589–603. <https://doi.org/10.1111/jnc.14990>
- Hansen, B. (2020). Diffusion kurtosis imaging as a tool in Neurotoxicology. *Neurotoxicity Research*, *37*(1), 41–47. <https://doi.org/10.1007/s12640-019-00100-3>
- Hansen, B., Khan, A. R., Shemesh, N., Lund, T. E., Sangill, R., Eskildsen, S. F., Østergaard, L., & Jespersen, S. N. (2017). White matter biomarkers from fast protocols using axially symmetric diffusion kurtosis imaging. *NMR in Biomedicine*, *30*(9), e3741. <https://doi.org/10.1002/nbm.3741>
- Hansen, B., Lund, T. E., Sangill, R., & Jespersen, S. N. (2013). Experimentally and computationally fast method for estimation of a mean kurtosis. *Magnetic Resonance in Medicine*, *69*(6), 1754–1760. <https://doi.org/10.1002/mrm.24743>
- Harrop, C., Jones, D., Zheng, S., Nowell, S. W., Boyd, B. A., & Sasson, N. (2018). Sex differences in social attention in autism spectrum disorder. *Autism Research*, *11*(9), 1264–1275. <https://doi.org/10.1002/aur.1997>
- Harvey, L., & Boksa, P. (2012). A stereological comparison of GAD67 and reelin expression in the hippocampal stratum oriens of offspring from two mouse models of maternal inflammation during pregnancy. *Neuropharmacology*, *62*(4), 1767–1776. <https://doi.org/10.1016/j.neuropharm.2011.11.022>
- Hazlett, H. C., Gu, H., Munsell, B. C., Kim, S. H., Styner, M., Wolff, J. J., Elison, J. T., Swanson, M. R., Zhu, H., Botteron, K. N., Collins, D. L., Constantino, J. N., Dager, S. R., Estes, A. M., Evans, A. C., Fonov, V. S., Gerig, G., Kostopoulos, P., McKinstry, R., ... Statistical Analysis. (2017). Early brain development in infants at high risk for autism spectrum disorder. *Nature*, *542*(7641), 348–351. <https://doi.org/10.1038/nature21369>
- Howson, C. P., Kinney, M. V., McDougall, L., & Lawn, J. E. (2013). Born too soon: Preterm birth matters. *Reproductive Health*, *10*(Suppl 1), S1. <https://doi.org/10.1186/1742-4755-10-s1-s1>
- Ichtchenko, K., Hata, Y., Nguyen, T., Ullrich, B., Missler, M., Moomaw, C., & Sudhof, T. C. (1995). Neuroligin 1: A splice site-specific ligand for beta-neurexins. *Cell*, *81*(3), 435–443. [https://doi.org/10.1016/0092-8674\(95\)90396-8](https://doi.org/10.1016/0092-8674(95)90396-8)
- Jensen, J. H., Helpert, J. A., Ramani, A., Lu, H., & Kaczynski, K. (2005). Diffusional kurtosis imaging: The quantification of non-gaussian water diffusion by means of magnetic resonance imaging. *Magnetic Resonance in Medicine*, *53*(6), 1432–1440. <https://doi.org/10.1002/mrm.20508>
- Kettenmann, H., Hanisch, U. K., Noda, M., & Verkhratsky, A. (2011). Physiology of microglia. *Physiological Reviews*, *91*(2), 461–553. <https://doi.org/10.1152/physrev.00011.2010>
- Kim, W., Im, M. J., Park, C. H., Lee, C. J., Choi, S., & Yoon, B. J. (2013). Remodeling of the dendritic structure of the striatal medium spiny neurons accompanies behavioral recovery in a mouse model of Parkinson's disease. *Neuroscience Letters*, *557*, 95–100. <https://doi.org/10.1016/j.neulet.2013.10.049>
- Krueger, D. D., Tuffy, L. P., Papadopoulos, T., & Brose, N. (2012). The role of neurexins and neuroligins in the formation, maturation, and function of vertebrate synapses. *Current Opinion in Neurobiology*, *22*(3), 412–422. <https://doi.org/10.1016/j.conb.2012.02.012>
- Kuhn, S. A., van Landeghem, F. K., Zacharias, R., Färber, K., Rappert, A., Pavlovic, S., Hoffmann, A., Nolte, C., & Kettenmann, H. (2004). Microglia express GABA(B) receptors to modulate interleukin release. *Molecular and Cellular Neurosciences*, *25*(2), 312–322. <https://doi.org/10.1016/j.mcn.2003.10.023>
- Kwon, H. B., Kozorovitskiy, Y., Oh, W. J., Peixoto, R. T., Akhtar, N., Saulnier, J. L., Gu, C., & Sabatini, B. L. (2012). Neuroligin-1-dependent competition regulates cortical synaptogenesis and synapse number. *Nature Neuroscience*, *15*(12), 1667–1674. <https://doi.org/10.1038/nn.3256>

- Lai, J. K., Doering, L. C., & Foster, J. A. (2016). Developmental expression of the neuroligins and neuroligins in fragile X mice. *Journal of Comparative Neurology*, 524(4), 807–828. <https://doi.org/10.1002/cne.23868>
- Lammert, D. B., & Howell, B. W. (2016). RELN mutations in autism Spectrum disorder. *Frontiers in Cellular Neuroscience*, 10, 84. <https://doi.org/10.3389/fncel.2016.00084>
- Lee, G. H., & D'Arcangelo, G. (2016). New insights into Reelin-mediated signaling pathways. *Frontiers in Cellular Neuroscience*, 10, 122. <https://doi.org/10.3389/fncel.2016.00122>
- Li, G., Chen, M. H., Li, G., Wu, D., Lian, C., Sun, Q., Shen, D., & Wang, L. (2019). A longitudinal MRI study of amygdala and hippocampal subfields for infants with risk of autism. Graph Learning in Medical Imaging: First International Workshop, GLMI 2019, Held in Conjunction with MICCAI 2019, Shenzhen, China, October 17, 2019, Proceedings, 11849, 164–171. [https://doi.org/10.1007/978-3-030-35817-4\\_20](https://doi.org/10.1007/978-3-030-35817-4_20)
- Lilley, E., Stanford, S. C., Kendall, D. E., Alexander, S. P., Cirino, G., Docherty, J. R., George, C. H., Insel, P. A., Izzo, A. A., Ji, Y., Panettieri, R. A., Sobey, C. G., Stefanska, B., Stephens, G., Teixeira, M., & Ahluwalia, A. (2020). ARRIVE 2.0 and the *British Journal of Pharmacology*: Updated guidance for 2020. *British Journal of Pharmacology*. <https://doi.org/10.1111/bph.15178>
- Lim, S. T., Chang, A., Giuliano, R. E., & Federoff, H. J. (2012). Ectodomain shedding of nectin-1 regulates the maintenance of dendritic spine density. *Journal of Neurochemistry*, 120(5), 741–751. <https://doi.org/10.1111/j.1471-4159.2011.07592.x>
- Lim, S. T., Lim, K. C., Giuliano, R. E., & Federoff, H. J. (2008). Temporal and spatial localization of nectin-1 and I-afadin during synaptogenesis in hippocampal neurons. *Journal of Comparative Neurology*, 507(2), 1228–1244. <https://doi.org/10.1002/cne.21608>
- Little, L. M., Wallisch, A., Salley, B., & Jamison, R. (2017). Do early caregiver concerns differ for girls with autism spectrum disorders? *Autism*, 21(6), 728–732. <https://doi.org/10.1177/1362361316664188>
- Logiaccio, F., Xia, P., Georgiev, S. V., Franconi, C., Chang, Y. J., Ugursu, B., Sporbert, A., Kühn, R., Kettenmann, H., & Semtner, M. (2021). Microglia sense neuronal activity via GABA in the early postnatal hippocampus. *Cell Reports*, 37(13), 110128. <https://doi.org/10.1016/j.celrep.2021.110128>
- Malkova, N. V., Yu, C. Z., Hsiao, E. Y., Moore, M. J., & Patterson, P. H. (2012). Maternal immune activation yields offspring displaying mouse versions of the three core symptoms of autism. *Brain, Behavior, and Immunity*, 26(4), 607–616. <https://doi.org/10.1016/j.bbi.2012.01.011>
- Mallya, A. P., Wang, H. D., Lee, H. N. R., & Deutch, A. Y. (2019). Microglial pruning of synapses in the prefrontal cortex during adolescence. *Cerebral Cortex*, 29(4), 1634–1643. <https://doi.org/10.1093/cercor/bhy061>
- Mandai, K., Rikitake, Y., Mori, M., & Takai, Y. (2015). Nectins and nectin-like molecules in development and disease. *Current Topics in Developmental Biology*, 112, 197–231. <https://doi.org/10.1016/bs.ctdb.2014.11.019>
- McNaught, A. (1997). In A. D. McNaught & A. Wilkinson (Eds.), *Compendium of chemical terminology*. Blackwell Scientific Publications.
- Megias, M., Emri, Z., Freund, T. F., & Gulyas, A. I. (2001). Total number and distribution of inhibitory and excitatory synapses on hippocampal CA1 pyramidal cells. *Neuroscience*, 102(3), 527–540. [https://doi.org/10.1016/s0306-4522\(00\)00496-6](https://doi.org/10.1016/s0306-4522(00)00496-6)
- Mizoguchi, A., Nakanishi, H., Kimura, K., Matsubara, K., Ozaki-Kuroda, K., Katata, T., Honda, T., Kiyohara, Y., Heo, K., Higashi, M., Tsutsumi, T., Sonoda, S., Ide, C., & Takai, Y. (2002). Nectin: An adhesion molecule involved in formation of synapses. *Journal of Cell Biology*, 156(3), 555–565. <https://doi.org/10.1083/jcb.200103113>
- Moore, T., Johnson, S., Hennessy, E., & Marlow, N. (2012). Screening for autism in extremely preterm infants: Problems in interpretation. *Developmental Medicine and Child Neurology*, 54(6), 514–520. <https://doi.org/10.1111/j.1469-8749.2012.04265.x>
- Nimchinsky, E. A., Sabatini, B. L., & Svoboda, K. (2002). Structure and function of dendritic spines. *Annual Review of Physiology*, 64, 313–353. <https://doi.org/10.1146/annurev.physiol.64.081501.160008>
- Niu, S., Renfro, A., Quattrocchi, C. C., Sheldon, M., & D'Arcangelo, G. (2004). Reelin promotes hippocampal dendrite development through the VLDLR/ApoER2-Dab1 pathway. *Neuron*, 41(1), 71–84. [https://doi.org/10.1016/s0896-6273\(03\)00819-5](https://doi.org/10.1016/s0896-6273(03)00819-5)
- Pelkey, K. A., Chittajallu, R., Craig, M. T., Tricoire, L., Wester, J. C., & McBain, C. J. (2017). Hippocampal GABAergic inhibitory interneurons. *Physiological Reviews*, 97(4), 1619–1747. <https://doi.org/10.1152/physrev.00007.2017>
- Percie du Sert, N., Hurst, V., Ahluwalia, A., Alam, S., Avey, M. T., Baker, M., Browne, W. J., Clark, A., Cuthill, I. C., Dirnagl, U., Emerson, M., Garner, P., Holgate, S. T., Howells, D. W., Karp, N. A., Lasic, S. E., Lidster, K., MacCallum, C. J., Macleod, M., ... Würbel, H. (2020). The ARRIVE guidelines 2.0: Updated guidelines for reporting animal research. *BMJ Open Science*, 4(1), e100115. <https://doi.org/10.1136/bmjos-2020-100115>
- Persico, A. M., D'Agruma, L., Maiorano, N., Totaro, A., Militeri, R., Bravaccio, C., Wassink, T. H., Schneider, C., Melmed, R., Trillo, S., Montecchi, F., Palermo, M., Pascucci, T., Puglisi-Allegra, S., Reichelt, K. L., Conciatori, M., Marino, R., Quattrocchi, C. C., Baldi, A., ... Collaborative Linkage Study of Autism. (2001). Reelin gene alleles and haplotypes as a factor predisposing to autistic disorder. *Molecular Psychiatry*, 6(2), 150–159. <https://doi.org/10.1038/sj.mp.4000850>
- Prosperi, M., Turi, M., Guerrera, S., Napoli, E., Tancredi, R., Iglizios, R., Apicella, F., Valeri, G., Lattarulo, C., Gemma, A., & Santocchi, E. (2020). Sex differences in autism Spectrum disorder: An investigation on core symptoms and psychiatric comorbidity in preschoolers. *Frontiers in Integrative Neuroscience*, 14, 62.
- Qvist, P., Eskildsen, S. F., Hansen, B., Baragji, M., Ringgaard, S., Roovers, J., Paternoster, V., Molgaard, S., Corydon, T. J., Stødkilde-Jørgensen, H., Glerup, S., Mors, O., Wegener, G., Nyengaard, J. R., Børsglum, A. D., & Christensen, J. H. (2018). Brain volumetric alterations accompanied with loss of striatal medium-sized spiny neurons and cortical parvalbumin expressing interneurons in Brd1(+/-) mice. *Scientific Reports*, 8(1), 16486. <https://doi.org/10.1038/s41598-018-34729-5>
- Rasmuson, A., Hahn, U., Larsen, J. O., Gundersen, H. J. G., Jensen, E. B. V., & Nyengaard, J. R. (2013). The spatial rotator. *Journal of Microscopy*, 250(2), 88–100. <https://doi.org/10.1111/jmi.12022>
- Ratnayake, U., Quinn, T., Walker, D. W., & Dickinson, H. (2013). Cytokines and the neurodevelopmental basis of mental illness. *Frontiers in Neuroscience*, 7, 180. <https://doi.org/10.3389/fnins.2013.00180>
- Raymond, G. V., Bauman, M. L., & Kemper, T. L. (1996). Hippocampus in autism: A Golgi analysis. *Acta Neuropathologica*, 91(1), 117–119. <https://doi.org/10.1007/s004010050401>
- Rikitake, Y., Mandai, K., & Takai, Y. (2012). The role of nectins in different types of cell-cell adhesion. *Journal of Cell Science*, 125(Pt 16), 3713–3722. <https://doi.org/10.1242/jcs.099572>
- Schumann, C. M., Hamstra, J., Goodlin-Jones, B. L., Lotspeich, L. J., Kwon, H., Buonocore, M. H., Lammers, C. R., Reiss, A. L., & Amaral, D. G. (2004). The amygdala is enlarged in children but not adolescents with autism; the hippocampus is enlarged at all ages. *The Journal of Neuroscience*, 24(28), 6392–6401. <https://doi.org/10.1523/JNEUROSCI.1297-04.2004>
- Seiple, B. D., Blomgren, K., Gimlin, K., Ferriero, D. M., & Noble-Haesslein, L. J. (2013). Brain development in rodents and humans: Identifying benchmarks of maturation and vulnerability to injury across species. *Progress in Neurobiology*, 106–107, 1–16. <https://doi.org/10.1016/j.pneurobio.2013.04.001>

- Shen, M. D., Nordahl, C. W., Young, G. S., Wootton-Gorges, S. L., Lee, A., Liston, S. E., Harrington, K. R., Ozonoff, S., & Amaral, D. G. (2013). Early brain enlargement and elevated extra-axial fluid in infants who develop autism spectrum disorder. *Brain*, 136(Pt 9), 2825–2835. <https://doi.org/10.1093/brain/awt166>
- Sholl, D. A. (1953). Dendritic organization in the neurons of the visual and motor cortices of the cat. *Journal of Anatomy*, 87(4), 387–406. Retrieved from <https://www.ncbi.nlm.nih.gov/pubmed/13117757>
- Smith, P. L., Hagberg, H., Naylor, A. S., & Mallard, C. (2014). Neonatal peripheral immune challenge activates microglia and inhibits neurogenesis in the developing murine hippocampus. *Developmental Neuroscience*, 36(2), 119–131. <https://doi.org/10.1159/000359950>
- Sparks, B. F., Friedman, S. D., Shaw, D. W., Aylward, E. H., Echelard, D., Artru, A. A., Maravilla, K. R., Giedd, J. N., Munson, J., Dawson, G., & Dager, S. R. (2002). Brain structural abnormalities in young children with autism spectrum disorder. *Neurology*, 59(2), 184–192. <https://doi.org/10.1212/wnl.59.2.184>
- Strunk, T., Inder, T., Wang, X., Burgner, D., Mallard, C., & Levy, O. (2014). Infection-induced inflammation and cerebral injury in preterm infants. *The Lancet Infectious Diseases*, 14(8), 751–762. [https://doi.org/10.1016/S1473-3099\(14\)70710-8](https://doi.org/10.1016/S1473-3099(14)70710-8)
- Sudhof, T. C. (2008). Neuroligins and neuexins link synaptic function to cognitive disease. *Nature*, 455(7215), 903–911. <https://doi.org/10.1038/nature07456>
- Tang, G., Gudsnuik, K., Kuo, S. H., Cotrina, M. L., Rosoklija, G., Sosunov, A., Sonders, M. S., Kanter, E., Castagna, C., Yamamoto, A., Yue, Z., Arancio, O., Peterson, B. S., Champagne, F., Dwork, A. J., Goldman, J., & Sulzer, D. (2014). Loss of mTOR-dependent macroautophagy causes autistic-like synaptic pruning deficits. *Neuron*, 83(5), 1131–1143. <https://doi.org/10.1016/j.neuron.2014.07.040>
- Taylor, M. J., Rosenqvist, M. A., Larsson, H., Gillberg, C., D'Onofrio, B. M., Lichtenstein, P., & Lundstrom, S. (2020). Etiology of autism Spectrum disorders and autistic traits over time. *JAMA Psychiatry*, 77(9), 936–943. <https://doi.org/10.1001/jamapsychiatry.2020.0680>
- Taylor, P. V., Veenema, A. H., Paul, M. J., Bredewold, R., Isaacs, S., & de Vries, G. J. (2012). Sexually dimorphic effects of a prenatal immune challenge on social play and vasopressin expression in juvenile rats. *Biology of Sex Differences*, 3(1), 15. <https://doi.org/10.1186/2042-6410-3-15>
- Tejada, M. I., Elcoroaristizabal, X., Ibarluzea, N., Botella, M. P., de la Hoz, A. B., & Ocio, I. (2019). A novel nonsense homozygous variant in the NLGN1 gene found in a pair of monozygotic twin brothers with intellectual disability and autism. *Clinical Genetics*, 95(2), 339–340. <https://doi.org/10.1111/cge.13466>
- Treccani, G., Ardalán, M., Chen, F., Musazzi, L., Popoli, M., Wegener, G., Nyengaard, J. R., & Müller, H. K. (2019). S-ketamine reverses hippocampal dendritic spine deficits in Flinders sensitive line rats within 1 h of administration. *Molecular Neurobiology*, 56(11), 7368–7379. <https://doi.org/10.1007/s12035-019-1613-3>
- Uppal, N., Puri, R., Yuk, F., Janssen, W. G., Bozdagi-Gunal, O., Harony-Nicolas, H., Dickstein, D. L., Buxbaum, J. D., & Hof, P. R. (2015). Ultrastructural analyses in the hippocampus CA1 field in Shank3-deficient mice. *Molecular Autism*, 6, 41. <https://doi.org/10.1186/s13229-015-0036-x>
- Vaags, A. K., Lionel, A. C., Sato, D., Goodenberger, M., Stein, Q. P., Curran, S., Ogilvie, C., Ahn, J. W., Drmic, I., Senman, L., Chrysler, C., Thompson, A., Russell, C., Prasad, A., Walker, S., Pinto, D., Marshall, C. R., Stavropoulos, D. J., Zwaigenbaum, L., ... Scherer, S. W. (2012). Rare deletions at the Neurexin 3 locus in autism Spectrum disorder. *American Journal of Human Genetics*, 90(1), 133–141. <https://doi.org/10.1016/j.ajhg.2011.11.025>
- VanRyzin, J. W., Marquardt, A. E., Argue, K. J., Vecchiarelli, H. A., Ashton, S. E., Arambula, S. E., Hill, M. N., & McCarthy, M. M. (2019). Microglial phagocytosis of newborn cells is induced by endocannabinoids and sculpt sex differences in juvenile rat social play. *Neuron*, 102(2), 435–449.e6. <https://doi.org/10.1016/j.neuron.2019.02.006>
- Vargas, D. L., Nascimbene, C., Krishnan, C., Zimmerman, A. W., & Pardo, C. A. (2005). Neuroglial activation and neuroinflammation in the brain of patients with autism. *Annals of Neurology*, 57(1), 67–81. <https://doi.org/10.1002/ana.20315>
- Varghese, M., Keshav, N., Jacot-Descombes, S., Warda, T., Wicinski, B., Dickstein, D. L., Harony-Nicolas, H., de Rubeis, S., Drapeau, E., Buxbaum, J. D., & Hof, P. R. (2017). Autism spectrum disorder: Neuropathology and animal models. *Acta Neuropathologica*, 134(4), 537–566. <https://doi.org/10.1007/s00401-017-1736-4>
- Watson, R. E., Desesso, J. M., Hurtt, M. E., & Cappon, G. D. (2006). Postnatal growth and morphological development of the brain: A species comparison. *Birth Defects Research. Part B, Developmental and Reproductive Toxicology*, 77(5), 471–484. <https://doi.org/10.1002/bdrb.20090>
- Weidenheim, K. M., Goodman, L., Dickson, D. W., Gillberg, C., Rastam, M., & Rapin, I. (2001). Etiology and pathophysiology of autistic behavior: Clues from two cases with an unusual variant of neuroaxonal dystrophy. *Journal of Child Neurology*, 16(11), 809–819. <https://doi.org/10.1177/08830738010160110601>
- Werling, D. M., Parikshak, N. N., & Geschwind, D. H. (2016). Gene expression in human brain implicates sexually dimorphic pathways in autism spectrum disorders. *Nature Communications*, 7, 10717. <https://doi.org/10.1038/ncomms10717>
- Wynn, J. L., Neu, J., Moldawer, L. L., & Levy, O. (2009). Potential of immunomodulatory agents for prevention and treatment of neonatal sepsis. *Journal of Perinatology*, 29(2), 79–88. <https://doi.org/10.1038/jp.2008.132>
- Yang, M., Silverman, J. L., & Crawley, J. N. (2011). Automated three-chambered social approach task for mice. *Current Protocols in Neuroscience*, 56, 8–26. <https://doi.org/10.1002/0471142301.ns0826s56>
- Yuan, H. M., Wang, Q. M., Liu, Y. H., Yang, W., He, Y., Gusella, J. F., Song, J., & Shen, Y. (2018). A rare exonic NRXN3 deletion segregating with neurodevelopmental and neuropsychiatric conditions in a three-generation Chinese family. *American Journal of Medical Genetics Part B-Neuropsychiatric Genetics*, 177(6), 589–595. <https://doi.org/10.1002/ajmg.b.32673>
- Yushkevich, P. A., Piven, J., Hazlett, H. C., Smith, R. G., Ho, S., Gee, J. C., & Gerig, G. (2006). User-guided 3D active contour segmentation of anatomical structures: Significantly improved efficiency and reliability. *NeuroImage*, 31(3), 1116–1128. <https://doi.org/10.1016/j.neuroimage.2006.01.015>
- Zhang, H., Liu, X., Zhang, C., Mundo, E., Maciardi, F., Grayson, D. R., Guidotti, A. R., & Holden, J. J. A. (2002). Reelin gene alleles and susceptibility to autism spectrum disorders. *Molecular Psychiatry*, 7(9), 1012–1017. <https://doi.org/10.1038/sj.mp.4001124>

## SUPPORTING INFORMATION

Additional supporting information may be found in the online version of the article at the publisher's website.

**How to cite this article:** Ardalán, M., Chumak, T., Quist, A., Hermans, E., Hoseinpoor Rafati, A., Gravina, G., Jabbari Shiadeh, S. M., Svedin, P., Alabaf, S., Hansen, B., Wegener, G., Westberg, L., & Mallard, C. (2022). Reelin cells and sex-dependent synaptopathology in autism following postnatal immune activation. *British Journal of Pharmacology*, 179(17), 4400–4422. <https://doi.org/10.1111/bph.15859>